UNIVERSIDAD TECNICA
FEDERICO SANTA MARIA

Departamento de Electrónica

DOCTORAL DISSERTATION

LINEAR GENERATOR DRIVE BASED ON MODULAR MULTILEVEL CONVERTER FOR WAVE ENERGY APPLICATIONS.

HENRY MAURICIO ZAPATA FONSECA

DOCTORATE PROGRAM
DOCTORATE IN ELECTRONIC ENGINERING

THESIS SUPERVISOR	:	PROF. DR. MARCELO PÉREZ LEIVA
EVALUATION COMMITTEE	:	PROF. DR. CHRISTIAN A. ROJAS
	:	PROF. DR. CARLOS R. BAIER

November 2023

A mi familia . . .

Agradezco a mi familia por su apoyo incondicional.

Acknowledgements

"Success is not final, failure is not fatal, it's the courage to continue that counts." - Winston Churchill.

I wish to thank my friends and colleagues at Advanced Center for Electrical and Electronic Engineering (AC3E) for my valuable and memorable time there. I owe special thanks to Professor Marcelo Pérez, with whom I enjoyed working. I am also grateful to those colleagues who have contributed to an enjoyable and motiving atmosphere at work during these years. Finally, my warmest thanks go to my family for their unconditional support.

RESUMEN

Si no se aplican medidas políticas contundentes, se prevé que en pocas décadas el mundo se enfrente simultáneamente a una escasez de energía y a una crisis climática, ambas derivadas de nuestra fuerte dependencia de los combustibles fósiles. La extracción sostenible de fuentes de energía renovables y el avance de las tecnologías para aprovecharlas son componentes esenciales de las estrategias de reducción de emisiones y de la garantía de un suministro energético estable.

La energía de las olas es una valiosa fuente de energía con una concentración de potencia relativamente alta y fácilmente accesible en las regiones costeras. Este recurso es lo suficientemente importante como para contribuir a la cartera energética global en determinadas zonas. Aunque la tecnología para aprovechar la energía de las olas del mar sigue en fase de investigación y desarrollo, el principal obstáculo reside en el diseño de sistemas cuyos costes están asociados a la inversión, el funcionamiento y el mantenimiento.

Esta tesis propone un convertidor multinivel modular (MMC) para controlar un generador lineal tubular de imanes permanentes (TPMLG) para un sistema de conversión de energía undimotriz (WEC). Se aplica un método de parámetros globales para analizar la amplitud de la tensión inducida y el campo magnético del TPMLG. Se emplea un análisis de elementos finitos en el software de simulación para obtener el comportamiento dinámico de estas variables. El MMC propuesto controla cada devanado del TPMLG de forma independiente; el MMC permite diseñar un MPPT que controlará el par en función de la altura de ola y tendrá un alto voltaje para mejorar la eficiencia de transmisión de energía a la costa. Los resultados experimentales y de simulación se validarán con un prototipo de laboratorio diseñado con las limitaciones y restricciones analizadas matemáticamente. El objetivo principal del trabajo de tesis propuesto es la mejora de la eficiencia de captación de energía, maximizando la energía transmitida desde los sistemas WEC a la estación costera.

Palabras claves:

- Convertidor de energía de olas
- Generador lineal
- Convertidor modular miltinivel

ABSTRACT

If robust political measures are not implemented, it is projected that in a few decades, the world will confront a simultaneous shortage of energy and a climate crisis, both of which stem from our heavy reliance on fossil fuels. The sustainable extraction of renewable energy sources and the advancement of technologies to harness them are essential components of emission reduction strategies and ensuring a stable energy supply.

Wave energy is a valuable energy source with a relatively high power concentration and is easily accessible in coastal regions. This resource is substantial enough to contribute to the overall energy portfolio in certain areas. Although the technology for harnessing the power of ocean waves is still under research and development, the main obstacle lies in designing systems where the costs are associated with investment, operation, and maintenance.

This thesis proposes a modular multilevel converter (MMC) to control a tubular permanent magnet linear generator (TPMLG) for a wave energy conversion (WEC) system. A lumped parameter method is applied to analyze the amplitude of induced voltage and the magnetic field of the TPMLG. A finite element analysis is employed in the simulation software to obtain the dynamical behavior of these variables. The proposed MMC controls each winding of the TPMLG independently; the MMC permits designing an MPPT that will control the torque in function to the wave height and have a high voltage to improve the energy transmission efficiency to the coast. The simulation and experimental results will be validated with a laboratory prototype designed with the limitations and constraints analyzed mathematically. The main focus of the proposed thesis work is the improvement of energy harvesting efficiency, maximizing the energy transmitted from the WEC systems to the coast station.

Keywords:

- Wave energy converter (WEC)
- Linear generator
- Modular multilevel converter (MMC)

Contents

List of Tables

List of Figures

1 | INTRODUCTION

1.1 Ocean Energy

The development of alternative renewable energy sources, such as solar, wind, geothermal, and ocean energy, has been driven by the need to mitigate global warming. The global estimate of renewable energy produced by the end of 2020 was 37% of the total energy produced worldwide [42, 75], as shown in Figure 1.1.

In terms of ocean energy, there are six different sources, each with different technologies for conversion [74, 22]:

- **Ocean waves:** Ocean wave energy is generated by the potential and kinetic energy of water particles as a result of wind interaction with the ocean. Factors such as wind speed, wind duration, and the length of the ocean over which the wind blows determine the size and period of the waves. The most significant wave energy power levels occur off the west coasts of temperate continents. The total theoretical potential of wave energy is estimated to be $32,000\ TWh/year$, which is twice as much as the world electricity supply in 2008. The technical potential of wave energy will be less than this figure and will depend on advances in wave energy devices. The long-term distribution of wave energy could also be affected by potential changes in wind patterns due to climate change. Finally, various devices are used to measure waves, such as wave-measuring buoys, seabed-mounted probes, and satellite-based measurements.
- **Tidal Range:** Tides are regular changes in the height of the ocean caused by the gravitational and rotational forces between the earth, moon, and sun, combined with centrifugal and inertial forces. These tides are experienced differently in different parts of the world, with some locations experiencing one tide per day and others experiencing two high and two low tides per day. Tidal ranges can vary due to the position of the Earth, Moon, and Sun and can be affected by the shape of the ocean bed, shoreline geometry, and Coriolis acceleration. Tidal periodicities can resonate with the natural oscillatory frequencies of estuaries and bays, resulting in significantly increased tidal range. The text also notes that tidal range can be predicted with high accuracy, even centuries in advance and that the theoretical global tidal energy potential is about $3\ TW$, although only a fraction of this potential is likely to be exploited.
- **Tidal Streams:** Tidal currents are generated by horizontal water movement and can be modified by the topography of the seabed. Tidal currents are predictable and largely insensitive to the effects of climate change. The energy flux method is a widely used approach to assessing tidal currents' energy resource potential, where tidal currents' power density increases substantially with small increases in velocity. The UK, EU, Canada, and China have published tidal stream resource estimates. Over 106 good sites have been identified in Europe, mainly in the UK, with a technical potential of 48 TWh/yr. Commercially attractive sites have also been identified in Canada, the Republic of Korea, and New Zealand.
- **Ocean Currents:** Ocean Currents are generated by forces from wind-driven water, the earth's rotation, and thermohaline ocean circulation. The open ocean has low variability and continuous current flows that can drive present-day technologies. Large-scale ocean currents are concentrated in various regions, such as the western boundary currents, including the Agulhas/Mozambique Currents, the Kuroshio Current, the East

Australian Current, and the Gulf Stream. These currents offer sufficient current velocities to drive current technologies and improvements in turbine systems. The Florida Current of the Gulf Stream system has a technical potential of 25 GW, flowing strongly year-round as part of the North Atlantic Ocean subtropical gyre. The "MacArthur Workshop" recognized this potential for power generation from the Florida Current decades ago.

- **Ocean Thermal Energy Conversion:** Ocean thermal energy conversion is derived from temperature differences between the ocean surface and deep ocean waters (below $1,000m$). The ocean retains about 15% of the total solar input as thermal energy, with the temperature declining exponentially with depth due to the low thermal conductivity of seawater. Ocean thermal energy conversion (OTEC) plants require a minimum temperature difference of 20°C between surface water and water at a depth of 1,000 meters. Many tropical regions meet these temperature requirements, and the OTEC resource map shows a wide tropical area with a potential temperature difference greater than 20°C. OTEC is a continuously available renewable resource that could contribute to base-load power supply, although its energy density is low compared to wave and tidal current energy. The theoretical potential for OTEC is estimated to be between 30,000 and 90,000 TWh/yr, and up to 88,000 TWh/yr of power could be generated from OTEC without affecting the ocean's thermal structure. Climate change is unlikely to have a meaningful impact on the size of the global technical potential for OTEC.
- **Salinity Gradients:** Salinity Gradients are derived from the difference in the salt concentration between fresh water and river mouths water. Mixing freshwater and seawater can release energy as heat, which can be captured as pressure across a semi-permeable membrane and then converted into proper energy forms. This process, known as osmotic power, can be harnessed globally in all regions with a sufficient freshwater supply, with river mouths being the most appropriate. The technical potential for power generation from osmotic power was recently calculated as 1,650 TWh/yr, potentially generating base-load electricity if cost-effective technologies can be developed.

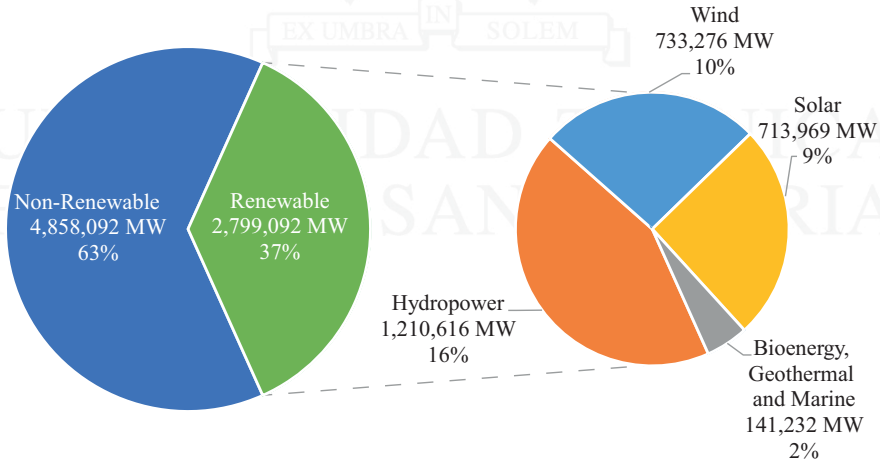

Figure 1.1: Estimated electricity installed capacity (MW). End 2020. The data were obtained from [42].

Ocean energy has significantly developed in recent years, although it is still less developed than wind and solar energy. The year 2021 ended approximately with $527MW$ of the operating capacity of ocean energy, corresponding to $3MW$ currently operational [42].

Wave energy has a great potential to generate electricity, considering that the estimation of total wave power on the coastlines is roughly $2TW$; furthermore, if wave energy is harvested on open oceans without loss in friction and wave breaking, then the estimation of global wave power input is up to $10TW$ [35, 59].

Table 1.1 shows the 12-year average annual ocean energy generation for all global points in the System Web GIS and shows the interest in producing this type of energy. The map in the figure Figure 1.2 clearly

shows that the most energy-rich areas of the global oceans are mid to high-latitude temperate storm belts of both hemispheres, particularly between 40^o and 60^o. The resources are much higher in the southern hemisphere, where seasonal variations are much lower [15].

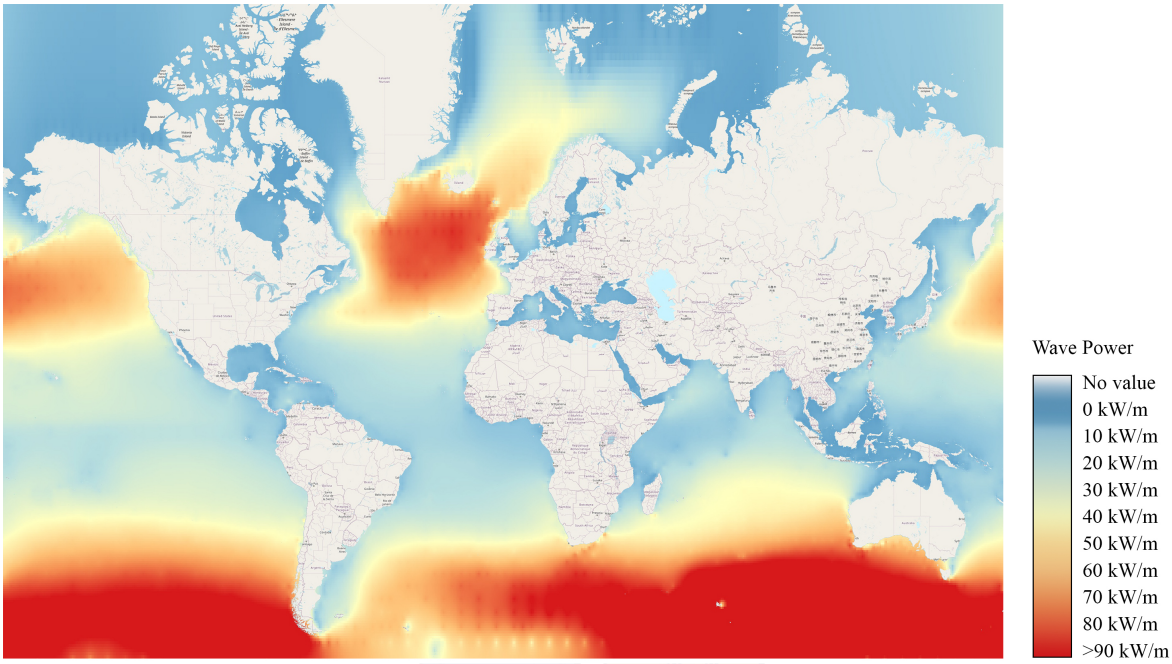

Figure 1.2: Global annual mean wave power estimates in kW/m (obtained from [3]).

Table 1.1: Ocean energy generation in different continents (MW), dataset by Irena [89].

	Years											
Continents	2009	2010	2011	2012	2013	2014	2015	2016	2017	2018	2019	2020
Africa	0	0	0	0	0	0	0	0	0	0	0	0
Asia	4	5	259	259	259	259	259	259	259	259	260	260
Europa	217	222	221	228	228	231	231	241	245	247	242	243
Oceania	1	1	1	1	1	1	1	1	1	1	1	1
Eurasia	2	2	2	2	2	2	2	2	2	2	2	2
America	20	20	20	20	20	20	20	20	20	20	20	20
World	244	250	503	509	510	513	513	519	523	527	525	527

Wave energy has two main advantages: Its a consistent and relatively predictable energy supply because many wave farm sites will receive a steady flow of waves, even when there are little or no local wind [42]. Wave energy is also easier to forecast than wind energy, allowing for better integration into power grids [69].

1.2 Wave Energy Converters

Wave Energy Converters (WECs) capture wave energy to convert it into electricity. They are less developed than solar or wind converters due to: the diversity of the wave resources in offshore and nearshore locations, which makes it difficult for the design to obtain high efficiency over an entire range of operations and the complexity of capturing the maximum energy without damage by the instability of the energy intensity [20, 17, 47, 74, 1].

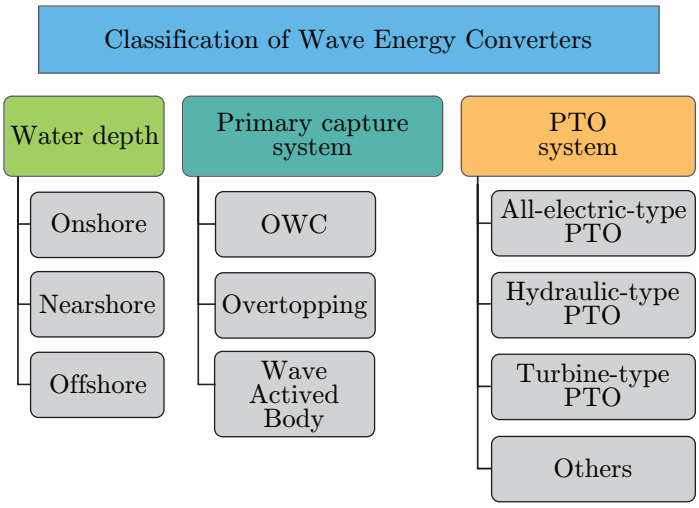

Figure 1.3: Classification of WECs according to different criteria.

A wide variety of WECs prototypes have been developed and can be classified by location, size, and energy absorption mechanisms [81], as shown in Figure 1.3:

1.2.1 Classification water depth

WECs can be classified by the ocean water-depth location in three categories, as shown in Figure 1.4:

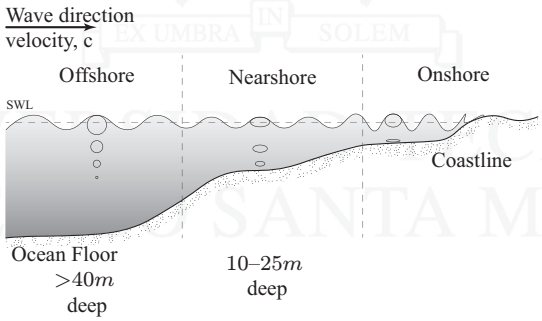

Figure 1.4: WEC classification according to location.

1. **Onshore devices** have the advantage of being close to the grid, easy to maintain, and reducing the likelihood of being damaged in extreme conditions. However, lower wave power is obtained. Tidal range can also be an issue [17].
2. **Nearshore devices** are defined as devices in relatively shallow water. Like shoreline devices, a disadvantage is that shallow water leads to waves with reduced power, limiting the harvesting potential [20, 17].
3. **Offshore devices** are located in deep waters (more than 40 m). Due to their location, they might exploit the vast wave power of the open sea. Long-length expensive sea cables are used to carry the energy to the grid [20, 66, 17].

It is useful to note that the energy in a wave is up to 95% between the water surface and a quarter wavelength below it [20].

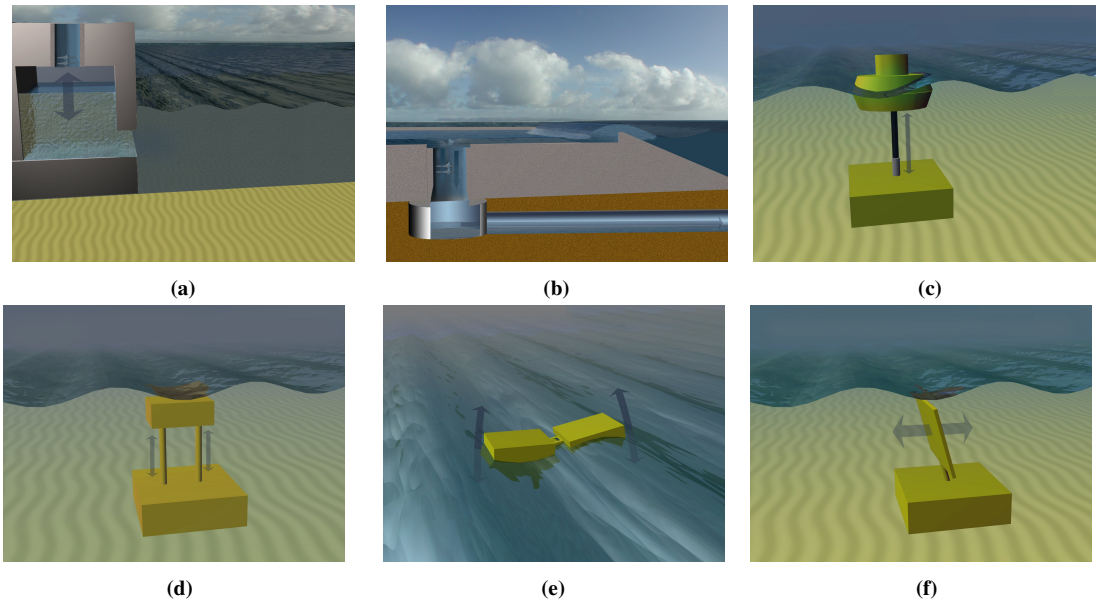

Figure 1.5: Main types of WEC, images from European Marine Energy Centre Ltd. [2]: a) Oscillating water column, b) Overtopping, c) Floating structure (Point absorber), d) Submerged pressure differential (Point absorber), e) Attenuator, f) Oscillating wave surge converter (Terminator).

1.2.2 Classification capture system

Depending on the primary capture system WECs can be categorized into oscillating water column (OWC) type, overtopping, and wave-activated body (WAB) [87, 55], as described in the following:

1. **Oscillating water column:** is a floating, or fixed hollow configuration open to the water below the surface [24]. An air pocket is alternatively compressed and expanded by the water column oscillations, as shown in Figure 1.5a. The confined air is forced to pass through a turbine, combined with an electrical generator [48]. Limpet, Mighty Whale, Oceanlinx, Osprey, and Pico plant are among the existing oscillating water column types of wave energy converters.
2. **Overtopping:** water from the incoming waves will overtop the structure, and it is then stored in the reservoir, which in turn, runs a turbine that generates electricity, as shown in Figure 1.5b. Sea-wave Slot-cone Generator (SSG), Tapchan, and Wave Dragon are among the existing overtopping system types of wave energy converters [59, 24, 40].
3. **Wave activated body:** The WAB can be subclassified into point absorbers, attenuators, and terminators.
    - Point absorber: These are small vertical devices either fixed directly to the ocean floor or tethered via a chain that absorbs the wave energy from all directions [23, 59], as shown in Figure 1.5c, 1.5d. For example, AquaBuoy (Canada), Archimedes Buoy (Scotland), BioWave (Australia), L10 Buoy (Sweden), OPT Power (USA), Pendulum (Japan), and SEAREV [14, 12, 80, 59, 70].
    - Attenuator: These structures are placed parallel to the wave direction. The wave-induced motion is used to pressurize a hydraulic piston, which forces high-pressure oil to turn a hydraulic turbine generator producing electricity [55, 59], an example is shown in Figure 1.5e.
    - Terminator: These devices are similar to attenuators. Nevertheless, they are placed perpendicular to the predominant direction of wave propagation [22, 55, 45], an example is shown in Figure 1.5f.

1.2.3 Classification by PTO

A Power take-off (PTO) has a moving element and a generator, which convert the captured wave energy into electricity. According to the device used to drive generators, there are three main groups: hydraulic, turbine and all-electric [87, 54].

1. The **hydraulic** PTO is robust and able to provide a large force at low speed, which coincides with characteristics of the ocean waves. Another advantage is that most of the components used in hydraulic circuits are commercially available. As shown in Figure 1.6a, their working principle is that ocean waves drive the hydraulic ram to increase the pressure by a compression unit, and the hydraulic energy drives a generator to produce electricity. Hydraulic PTOs are widely used for WECs, including the Pelamis, Wavebob, and Edinburgh Duck [79].
2. **Turbines** are also widely used for WECs, and they are driven by water or compressed air as shown in Figure 1.6b-c. A detailed introduction and comparison of turbines are made in [84, 87], indicating that impulse-type turbines are more suitable for irregular waves than Wells turbines. Generators are directly connected to those turbines to produce electricity.
3. In the **all-electric** PTO, the generators should adapt to the slow-motion of ocean waves and are generally directly connected to the absorber, as shown in Figure 1.6d. The generator can be the linear or rotating type, i.e., a linear permanent magnet generator (LPMG) or a rotating permanent magnet generator. The Uppsala University WEC and the AWS WEC use an LPMG [90, 91].

Another PTO exists that does not fall into these three categories. They use different mechanisms, such as piezoelectric materials, to convert ocean kinetic energy into electrical energy [44]. These WECs are not discussed here, as they are still scarce.

1.3 Problem Statement and Motivation

There are several initiatives promoted by the Chilean government to impulse the development of wave energy harvesting [56], as well as several prototypes already installed along the Chilean coast [50].

The diversity of the wave resources and the instability of energy intensity make the design of wave energy converter systems (WECs) very challenging [20, 17]. To overcome these difficulties, selecting technologies for generating electrical energy from capturing mechanical energy is a crucial aspect of the design [6]. In this regard, the combination of point absorbers, which harvest the energy from the motion of submerged or floating buoys [59], and linear generators, which provide high energy density and direct conversion [4], have proved to be highly efficient because the mechanical swinging movement is directly transformed into electrical energy. Several examples of linear generators used with point absorbers have been reported, such as the Seacap (France), Islandberg Project (Sweden), PowerBouy (New Jersey), InfinityWEC (Sweden), PowerPod (UK), among others [88].

Linear generators offer a simple and robust structure for electromagnetic conversion of a swinging movement [45]. A tubular permanent magnet linear generator (TPMLG) is a typical choice to harvest wave energy efficiently, and some shapes of permanent magnets (PMs) can optimize their properties, such as increasing flux linkage, reducing cogging force, or improving conversion efficiency [5, 16]. The PMs can be oriented using radial, axial, or Halbach configurations to modify the magnetic flux path for different translator-stator combinations [61]. The PMs are usually located in the translator, while a modular arrangement of the windings in the stator is usually employed to bring flexibility for easy sizing [39].

The power extracted from the waves depends on the operating frequency and is maximized when the frequency of the WEC matches the wave frequency [57]. There are several control strategies focused on extracting the maximum power from the wave, which can be classified depending on whether the control action to achieve resonance is imposed on the mechanical elements or the electromagnetic devices [86]. The search for the appropriate operating frequency is very challenging due to the irregular period and amplitude of the waves. The

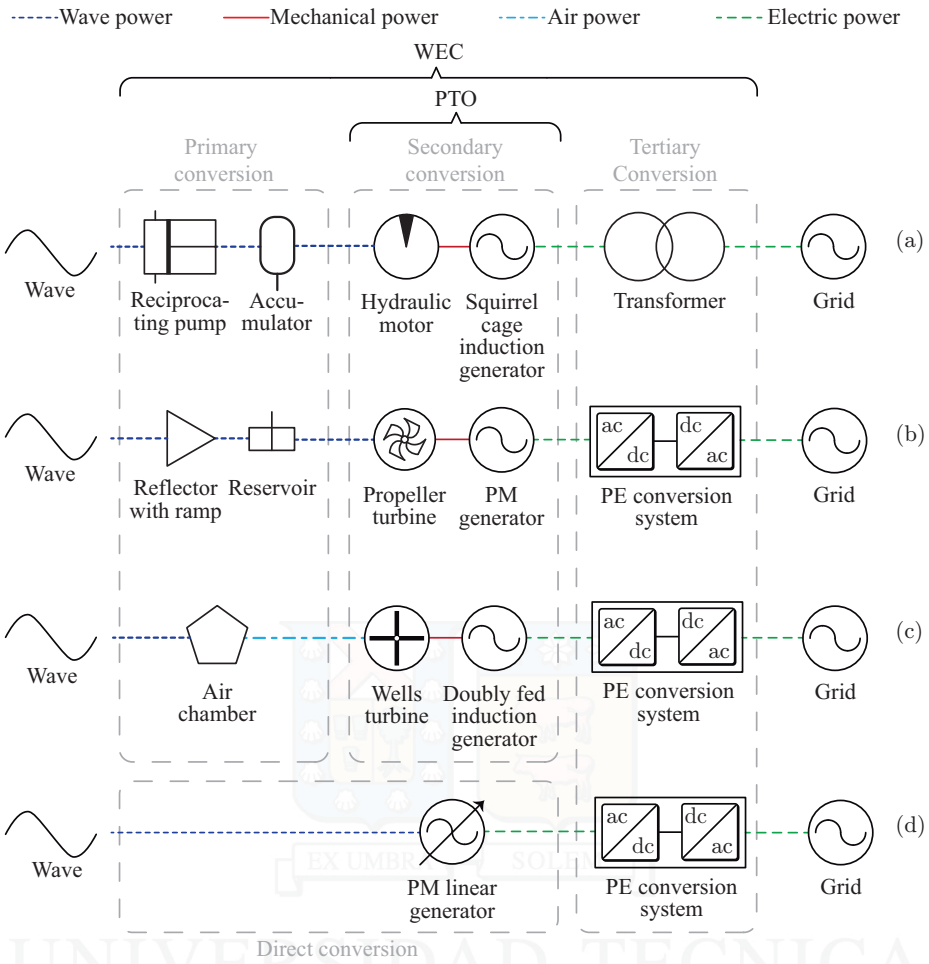

Figure 1.6: Technology used to produce electricity from wave. a) Hydraulic system, b) Wave Dragon device, c) Pico OWC device, d) Direct drive system.

wave period can be estimated using the velocity and acceleration information, but additional mechanical sensors are required for a precise estimation [68]. A passivity-based approach in which the velocity is associated with the wave energy can also be used to maximize the extracted energy [41]. On the other hand, a Hill-climbing algorithm, in which the electrical variables are slightly modified, and according to the power variation, the best operating condition is selected, provides good tracking performance without using additional sensors [93]. Multilevel converters based on submodules, such as the cascaded H-bridge and modular multilevel converter, allow the linear generator windings to be connected to different submodules, further increasing the energy harvesting by using separated Maximum Power Point Tracking (MPPT) [71].

High-voltage direct current (HVDC) and Medium Voltage Direct Current (MVDC) technologies are particularly well suited for submarine power transmission due to the reduced losses, no requirements for reactive power compensation, and lower costs than AC transmission [67, 36]. Multilevel converters produce higher voltages than two-level converters, generating a voltage waveform composed of several voltage levels [63], reaching MVDC and HVDC operation voltages [64]. Due to the high-quality waveforms, they do not require filters; hence, the power density is increased. This power density is a critical parameter in wave energy conversion systems due to the limited space inside the buoy [96].

1.4 Thesis overview

This thesis presents a wave energy converter based on a linear generator, a multilevel cascaded converter, and its control scheme. Each generator winding is connected to a submodule of the converter and controlled independently to operate at the maximum power point. The control loop at the input side of the submodule maximizes the extracted power from the linear generator, and due to the independent connection of each submodule, the extracted power could be different, leading to the unbalances of the capacitor voltages. A second control loop at the output side of the submodule is proposed to balance the capacitor voltages and generate the output voltage. Both controllers are tested experimentally, demonstrating their performance. This alow to generate an MVDC to transmit energy to the coast to improve efficiency in the transmission.

1.5 Hypothesis

A modular multilevel converter can drive a linear generator with independent coils to improve the energy harvesting of WECs by controlling the magnetic flux and torque depending on the translator position. The proposed converter can work with a small voltage in each cell, but connecting cells in series can generate a high voltage and increase power transmission efficiency to coast.

1.6 Objectives

Develop a novel modular multilevel converter topology with its control to improve the energy harvesting and direct conversion efficiency of a WEC system based on a TPMLG.

Specific objectives

1. State of the art of wave energy, linear generators, MPPT, and modular multilevel converters.
2. Modeling and simulation of a TPMLG and the modular multilevel converter.
3. Design of a control strategy for current in the MMC, flux and torque of a linear drive, with an analysis of power oscillations.
4. Design and construction of a simulation prototype modular multilevel converter.
5. Validation of theoretical and simulation results.
6. Scientific diffusion of results in conferences and journals of the specialty.

1.7 Contributions

The research work presented in this chapter is extended and detailed in:

- **"Model of a permanent magnet linear generator"**: In this research paper, a tubular permanent magnet linear generator (TPMLG) is introduced as a potential wave energy converter. The TPMLG consists of an array of permanent magnets and independent coils. Both experimental and simulated data are utilized to evaluate the advantages and disadvantages of the proposed device. The amplitude of induced voltage and magnetic field is mathematically analyzed using a lumped parameter method, while a finite element analysis in simulation software is used to study the dynamical behavior of these variables. The performance of the TPMLG is tested at three different speeds, and a physical prototype is constructed to validate the theoretical analysis and simulations. Both the experimental and simulated results support the mathematical relationship between speed and induced voltage. [94]
- **"Control of Cascaded Multilevel Converter for Wave Energy Applications"**: This research paper introduces a control strategy for a wave energy conversion system that utilizes a linear generator and a

cascaded multilevel converter. The mechanical conversion system consists of a buoy directly linked to a linear generator. The windings of the generator are individually controlled by a cascaded multilevel power converter, implementing independent maximum power point tracking to optimize energy harvesting. The cascaded converter's output is regulated to maintain balanced DC capacitors and generate a multilevel voltage at the output terminals, reducing losses in the underwater transmission line. Experimental results demonstrate the effectiveness of the proposed control scheme, maximizing power generation by synchronizing the current with the induced voltage waveform and ensuring DC capacitor balance. [96]

- **"Modular Multilevel Converter for a Linear Generator for Wave Energy Converter"**: In this research, we propose the implementation of a modular multilevel converter for a linear generator in a wave energy converter. The individual control of the coils in this generator is employed to enhance the energy harvesting efficiency. This converter topology is divided into two stages. The initial stage utilizes a full-bridge to regulate the harvested current based on a reference generated through an MPPT method. The subsequent stage utilizes a half-bridge to control the DC-link voltage and the output current. Moreover, employing multilevel modular converters enables the generation of an intermediate DC voltage, which significantly reduces losses in energy transmission lines from offshore to a common coupling point on the shore.[95]

1.8 Outline of the Thesis

The thesis aims to comprehensively analyze the linear generator drives and modular multilevel converters to harvest wave energy.

Chapter 1: The objective of this chapter is to present the problem statement, provide the context and motivation behind the research, and outline the primary contributions that have been made.

Chapter 2: This chapter aims to collect and review the main contributions regarding wave energy converters to establish the main links, lineal generators, and modular multilevel converters to work in this thesis. It also includes the WECs classification according to characteristics and steps conversion. Also, a description of Maximum power point tracking and modular multilevel converter is added.

Chapter 3: The objective of this chapter is to tackle two challenges, namely "The mathematical model" and "Control strategy." Within this framework, the chapter presents a characterization of wave buoy interaction by utilizing the equation of motion, which provides essential technical information about the proposed system. Furthermore, it delves into the theoretical analysis of the modular multilevel converter (MMC) and its corresponding control strategy.

Chapter 4: The primary objective of this chapter is to focus on developing the simulation model and provide a comprehensive analysis of the system performance and corresponding simulated results. In addition, the chapter includes an exploration of energy harvesting methods for a farm wave energy converter (WEC), with particular emphasis on the positioning of the WECs.

Chapter 5: In this chapter, the setup implementation of the proposed system, which incorporates an emulated linear generator and the topology of the multilevel converter, is thoroughly discussed.

Chapter 6: This chapter comprehensively summarizes the overarching findings and conclusions derived from this research endeavor.

2 | LITERATURE REVIEW

2.1 Energy Conversion Stages

Multiple methods are available to extract power from waves, including pneumatic, hydraulic, and mechanical approaches. These various means of harnessing energy are commonly referred to as Take-Off systems; these systems can be divided into several stages based on the different conversions involved in obtaining the appropriate signal for grid injection.

The process of conversion from wave energy to electric power can be divided into three stages: primary conversion (capture system), secondary conversion (PTO system), and tertiary conversion (electric power conversion system) [55].

2.1.1 Primary conversion

This stage uses a pneumatic, hydraulic, or mechanical system to capture the wave energy as airflow, water flow, or body movement. The capturing efficiency of the irregular waves is a challenge to be managed with the device designed; for example, the oscillating water column captures the waves of the vertical movement, while the oscillating wave surge converter uses the pitching movement generated by the waves. Also, this stage should have a strong ability to capture wave energy and increase the low-frequency ($\sim 0.1Hz$) oscillatory motion waves. These structures can float or fix on the moorings[20, 55, 87].

2.1.2 Secondary Conversion

This stage involves converting energy from the working fluid generated in the previous step into electricity. The main elements used for this task are pneumatic and hydraulic turbines and electrical generators. Some of these power elements will be described in the following:

1. **Air-turbines:** conventional unidirectional air turbines are inappropriate in these devices. It uses rectifying valve systems to correct the flow direction or self-rectifying air turbines [48, 55]. The most relevant types are: Wells air-turbine, Dennis-Auld air-turbine, Impulse air-turbine
2. **Hydraulic turbines:** This technology is well established and has been used for many years in hydro-power generation plants [55, 77, 29, 11]. The two main types are Reaction hydro-turbine and Impulse hydro-turbine.
3. **High-pressure or oil-hydraulics cylinders:** These systems are generally used in slow oscillating bodies [66], like Aquabuoy [53], Pelamis, or PowerBuoy. The body motion is converted into hydraulic energy by a hydraulic cylinder and then electric energy using an electrical generator driven by a fast hydraulic motor. In order to store energy and ensure a consistent flow to the hydraulic motor for generating a steady power output, a gas or oil accumulator system is typically placed between the cylinder and the motor. This system stores energy over several wave periods.

4. **Electrical generator:** The electrical generator converts the mechanical energy produced by a central element into electrical energy to supply the electrical grid. Most generators are rotary, although linear generators have been developed for specific wave converters. Apart from the linear generator, various machines directly connected to a turbine are compared in [55, 40]. Although these studies focus on an OWC converter, they can also serve as a reference for other WECs. The following generators have been discussed in these works: Doubly Fed Induction Generator (DFIG), Squirrel Cage Induction Generator (SCIG), Field Wound Synchronous Generator (SG), Permanent Magnet Synchronous Generator (PMG).

2.1.3 Tertiary conversion

Power Converter Topology	Parts
a) 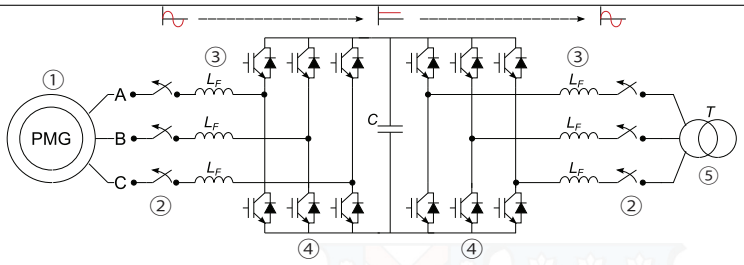	① Permanent magnet generator: rotatory or linear ② Main switches ③ Input and output filters ④ Input controller rectifier and output controller inverter in back-to-back configuration ⑤ Step-up transformer
b) 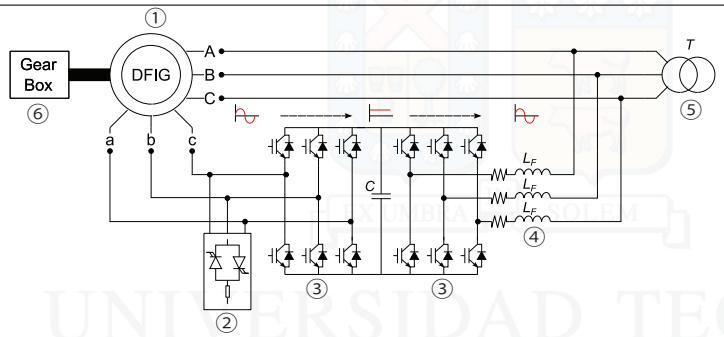	① Double fed induction generator ② Crowbar ③ Input rectifier and output inverter in back-to-back configuration ④ Output filter ⑤ Step-up transformer ⑥ Gear box
c) 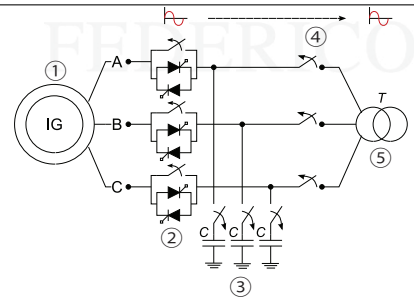	① Induction rotatory generator ② Soft start system ③ Reactive compensator ④ Main switches ⑤ Step-up transformer
d) 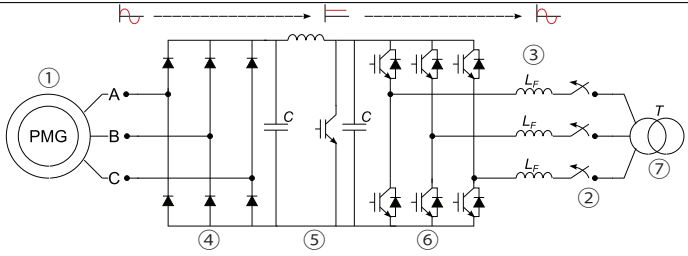	① Permanent magnet generator: rotatory or linear ② Main switches ③ Output filters ④ Input uncontrolled rectifier; diode bridge rectifier ⑤ Shunt ⑥ Controller inverter ⑦ Set-up transformer

Figure 2.1: Common power converters topologies used in wave energy converter devices, images from journal Renewable and Sustainable Energy Reviews [55].

This section is focused on the power electronic converter interfacing the generator and the power grid inside the WEC, delivering a fixed voltage and frequency waveform to the grid. The most common type of electronic converter employed in WECs is the three-phase Voltage Source Converter (VSC) due to its controllability, modular and compact design, and system interface easiness.

A back-to-back VSC can be used with a permanent magnet generator (PMG) either linear [60, 92, 8], or rotatory [14], as shown in Figure 2.1a. A DFIG generator with a gearbox coupled to a back-to-back power converter with a crowbar is often used in OWC converters [19, 52], as shown in Figure 2.1b. A squirrel-cage induction generator is directly connected to the grid, and a soft start system is proposed to reduce the inrush current during start-up, as shown in Figure 2.1c. The capacitor bank is installed to supply the required reactive current to the induction machine. This configuration is implemented in the Pelamis system [40]. An AC/DC diode bridge converter is employed instead of IGBT based AC/DC converter; therefore, the displacement of the generator current and voltage cannot be regulated, as shown in Figure 2.1d. There is a DC/DC regulator, in which the chopper controller controls the DC link voltage required for DC/AC conversion [76, 43]. The power converter usually has a step-up transformer connected to the output to raise the voltage level to an appropriate level for transport and connection to the grid.

2.2 Direct conversion

A linear generator is directly coupled to a vertical cylinder, which moves up and down with the incident sea wave in the direct conversion. This topology does not need the intervention of other mechanical systems. There are three main topologies of linear electrical generators: longitudinal flux permanent magnet generators, variable reluctance permanent magnet generators, and tubular air-cored permanent magnet generators [10].

The Back-to-Back converter is chosen due to its active rectifier on the generator side, which allows field-oriented control (FOC) and a complete decoupling between the generator and grid. The FOC is a high-performance machine drive strategy widely used with other technologies. This vector control allows very fast dynamic control of the machine, which is crucial to achieving the maximum generation of available energy through an MPPT. The power semiconductor devices used by the converter are IGBTs, which are switched by pulse width modulation (PWM).

2.2.1 Control strategies for direct conversion system

The direct drive system with a linear generator consists of a magnetic translator driven to reciprocate synchronously with a body directly coupled to a buoy. A simplified direct drive conversion system structure is shown in Figure 1.6a. Directly driven systems do not require an intermediate mechanical interface, thus avoiding the losses in turbines and hydraulic motors of other PTO systems. On the other hand, linear electrical generators for wave energy applications need power electronics to convert the generated electricity to a suitable form for the electric grid. Table 2.1 gives a summary of the control strategies [40].

2.2.2 Maximum power point tracking (MPPT)

Generally, renewable energy systems such as wind, solar, or marine energy face challenges due to variable weather conditions and their integration into the power grid. Wind and solar photovoltaic (PV) systems use Maximum Power Point Tracking (MPPT) techniques to optimize energy output. These techniques rely on an iterative approach implemented by the power converter, which adjusts the duty cycle to reach the MPPT point. This strategy remains effective even as the environmental conditions change, such as when operating at sea. However, this method may affect parameters such as current, voltage, or generator torque during the duty cycle calculation [62].

The actuator must be controlled to maximize the maximum available power in the waves. The force made by the translator (buoy) and k_s the WEC spring constant implies the floater is in resonance to extract the maximum power, in Equation 2.1. In other conditions, the force applied by the generator equals the force

Table 2.1: This summarizes example control strategies for direct conversion of point absorbers [40].

Control Strategy	Description
Resonant circuit	To achieve electric resonance with the generator windings.
Feedback linearization control	To cancel the non-linear dynamics of the generator in order to achieve closed-loop linear control.
Reactive control	Control the output impedance to be equal to the complex conjugate of the intrinsic impedance of the generator.
Phase and amplitude control	Control the floater vertical velocity in phase with wave excitation force, and the amplitude is regulated.
Latching control	Control the water damper to prevent the floater from moving.
Stiffness and damping control	Current control in the $dq0$ frame to control the active and reactive power respective stiffness and damping factor.
Vector control of PADA system	Control the generated current phase to be 90^o ahead of the flux inside the generator.

waves implying that the hydrodynamic damping is equal to the generator damping to harvest the maximum amount of energy in Equation 2.2. The water coefficient varies depending on sea waveforms, so it has to be continuously estimated. The maximization point is achieved through the active rectifier, which regulates the current and, consequently, the generator power. Better control over the MPPT is achieved by working on the physical design of the PTO, and its resonance frequency, which is omitted when establishing an open circuit fixed-voltage waveform for the linearized model [38, 72].

$$m_{tot}\frac{dv}{dt} + k_s h = 0 \,, \tag{2.1}$$

$$\beta_h = \beta_g \,, \tag{2.2}$$

where,

m_{tot} floater mass and an added mass representing the water above a floater that has to be accelerated;
k_s spring constant of the WEC.
v velocity of displacement of the WEC;
h position in axis vertical;
β_h hydrodynamic damping coefficient of the WEC;
β_g damping coefficient provided by the generator.

Figure 2.2 shows the maximum power point and illustrates the simplicity of the P&O MPPT method implementation.

2.2.3 Existing wave projects

The first WECs to be deployed were the $750kW$ Pelamis based on oscillating bodies (terminator) concept by the Pelamis Wave Power and the $250kW$ AWS based on oscillating bodies (point absorber) concept installed in Portugal in 2004. Some point absorbers with direct drive technologies are deployed in various projects worldwide, such as PB3 Powerbouy, Archimedes wave swing, and Seacap.

- **PB3 POWERBUOY:** OPT PB3 can act as an Uninterruptable Power Supply (UPS), which constantly recharges itself by harvesting energy from the waves. It is ocean-deployed, moored, and floats over the point of use and can operate in any ocean depth over $20m$ and up to $3,000m$. This WEC has a height of $13.3m$, spar diameter of $1m$, float diameter of $2.65m$, and produces an average power of $7.5kw$.

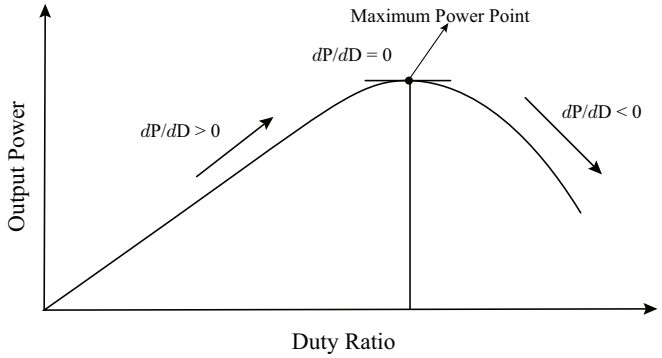

Figure 2.2: Schematic diagram of P&O (Perturb and Observe) curve of generation system.

- **Archimedes wave swing:** The AWS is a unique wave energy conversion system because it is completely submerged. It is important because this makes the system less vulnerable to storms. The high water pressure reduces the AWS volume. When a wave trough is above the AWS, the volume increases because of the air pressure inside the AWS. This linear motion can extract and convert energy into electrical energy.
- **Seacap:** It is a point absorber system for water depth from 20m to 50m; another version will be derived later for deeper horizons. A buoy absorbs the vertical motion of ocean waves. It floats around a column fixed to the seabed, capturing and transferring the waves' kinetic energy to linear electric generators. The modular nature system emphasizes safety and reliability, maintenance and performance, and survivability in extreme weather.

2.3 Modular Multilevel Converter

The voltage source converter (VSC) features are attractive to meet many challenges in medium-voltage applications; the more representative features are the generation of leading and lagging reactive power, high power density (MVA / per unit area), and fast dynamic response. An option to overcome the limitations is to directly connect semiconductor elements or converters in a series to create valves capable of withstanding higher voltages [46, 26, 34].

Instead, transitioning to multilevel converter topologies offers better prospects for cost-effective power conversion at higher voltages. These topologies do not require a direct series connection to increase the operating voltage. Furthermore, the harmonic properties are much improved to meet voltage, and current distortion requirements without excessive switching losses [78].

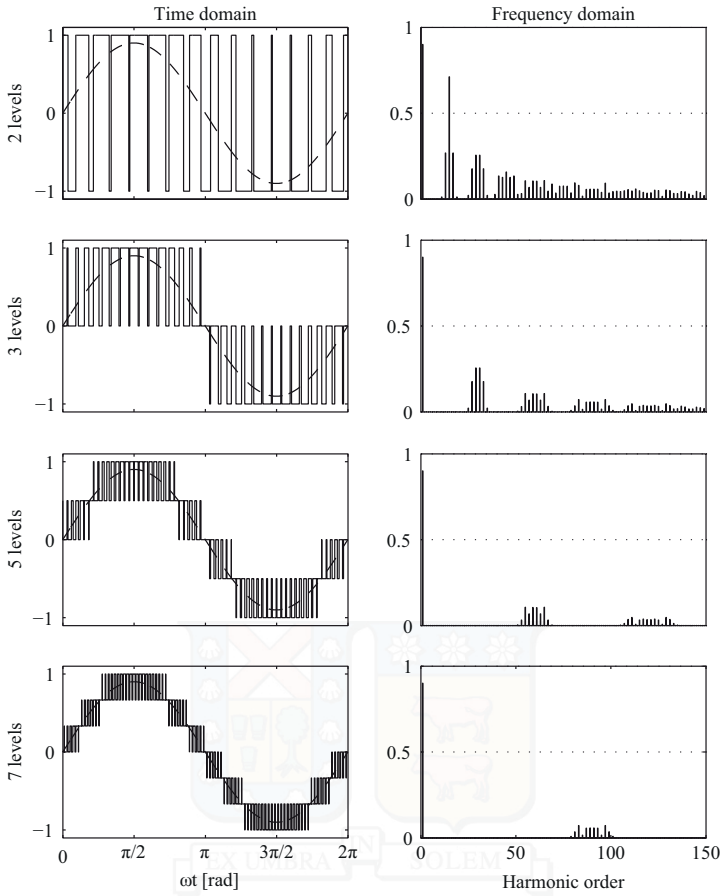

Figure 2.3: Impact of a transition to multilevel converters. The charts show the phase voltage of converters with two to seven levels in the time domain (left) and the frequency domain (right). [34].

The multilevel converter allows increased operating voltage without a series of switching devices. The advantages of a multilevel approach are [32]:

- Allows low voltage rated devices to generate medium or high voltage.
- Each switch device operates at a reduced switching frequency and experiences a small fraction of the total DC-link voltage. This results in low switching losses, audible noise, and dv/dt.
- Generates output voltage with low harmonic content, significantly reducing AC filtering.

The modular multilevel converter (MMC) has become the most attractive multilevel converter topology for medium/high-power applications, specifically for voltage-sourced converter high-voltage direct current (VSC–HVDC) transmission systems. In comparison with other multilevel converter topologies, the salient features of the MMC include [18]:

1. Modularity and scalability to meet any voltage level requirements.
2. High efficiency, which is of significant importance for high-power applications.
3. Superior harmonic performance, specifically in high-voltage applications where a large number of identical submodules (SMs) with low-voltage ratings are stacked up, thereby the size of passive filters can be reduced.
4. Absence of dc-link capacitors.

The MMC is better than the two-level converter due to the following features: improved efficiency, lower voltage and current on the switching devices, extremely low dv/dt, and audible noise resulting from small voltage steps and low switching frequency per device. These results confirm the suitability of the multilevel converter, such as M2C, for medium and high-voltage applications, such as reactive power compensation, medium voltage drive systems, interface for renewable power plants using wind and solar energy, high voltage dc transmission systems [34].

Figure 2.4(a) shows a schematic diagram of a three-phase MMC with two arms per phase leg where each arm comprises N series-connected, nominally identical SMs and a series inductor Lo. While the SMs in each arm are controlled to generate the required ac phase voltage, the arm inductor suppresses the high-frequency components in the arm current. The upper (lower) arm of three phase-legs is represented by subscript "p" ("n").

2.3.1 MMC Topology

The following circuits can realize the SMs of the MMC:

- The half-bridge circuit: As shown in Figure 2.4(b), the output voltage of a half-bridge SM is either equal to its capacitor voltage v_C (switched on/inserted state) or zero (switched-off/bypassed state), depending on the switching states of the complimentary switch pairs [58, 7, 85].
- The full-bridge circuit: As shown in Figure 2.4(c), the output voltage of a full-bridge SM is either equal to its capacitor voltage v_C (switched-on/inserted state) or zero (switched-off/bypassed state), depending on the switching states of the four switches $S1$ to $S4$. Since the number of semiconductor devices of a full-bridge SM is twice that of a half-bridge SM, the power losses, as well as the cost of an MMC based on the full-bridge SMs, are significantly higher than that of an MMC based on the half-bridge SMs [58, 7, 85].
- The clamp-double circuit: As shown in Figure 2.4(d), a clamp-double SM consists of two half-bridge SMs, two additional diodes, and one extra integrated gate bipolar transistor (IGBT) with its anti-parallel diode. During normal operation, the switch S5 is always switched ON, and the clamp-double SM acts equivalent to two series-connected half-bridge SMs. Compared to the half- and full-bridge MMCs with the same voltage levels, the clamp-double MMC has higher semiconductor losses than the half-bridge MMC, and lower than the full-bridge MMC [58].
- The three-level converter circuit: As shown in Figure 2.4(e) and (f), a three-level SM is comprised of either a three-level neutral-point-clamped (NPC) or a three-level flying capacitor (FC) converter. The three-level FC MMC has similar semiconductor losses to the half-bridge MMC. However, the three-level NPC MMC has higher semiconductor losses than the half-bridge MMC and lower than the full-bridge MMC. From a manufacturing perspective and control, this SM circuit is not very attractive [82, 83].
- The five-level cross-connected circuit: As shown in Figure 2.4(g), a five-level cross-connected SM also consists of two half-bridge SMs connected back-to-back by two extra IGBTs with their anti-parallel diodes. Its semiconductor losses are the same as the clamp-double SM [65].

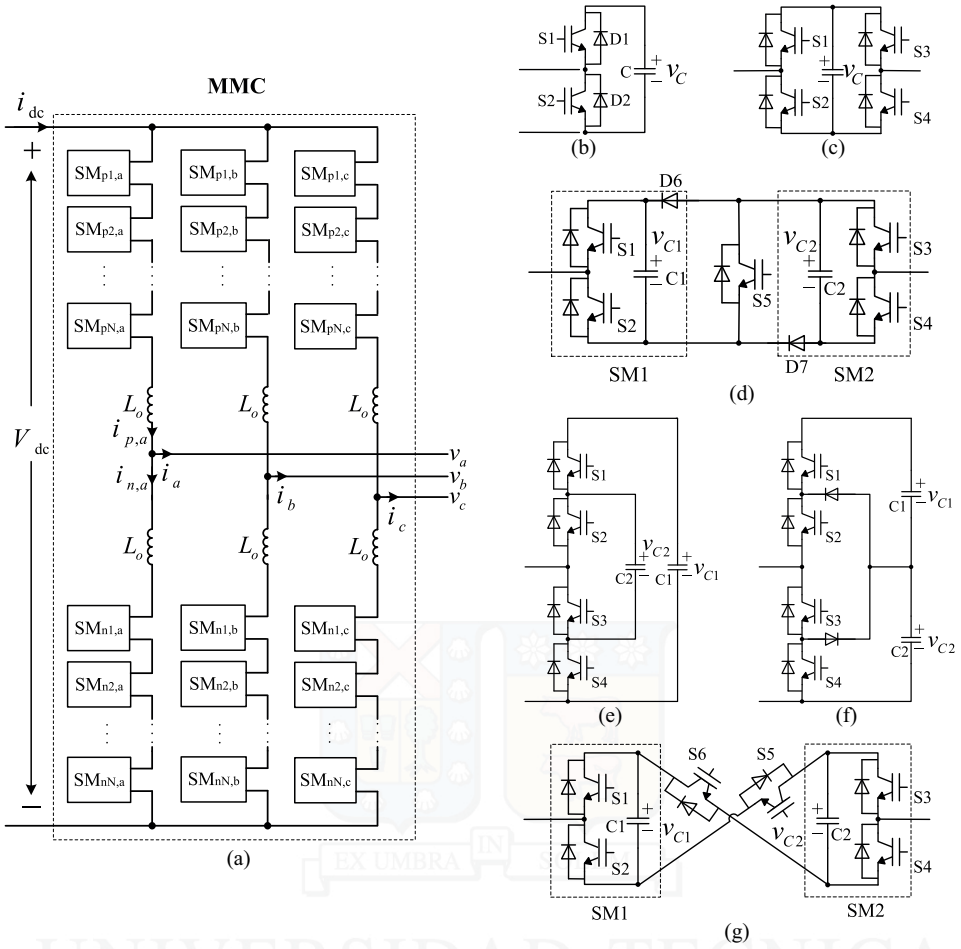

Figure 2.4: Schematic representation of a three-phase MMC and Various SM topologies: (a) Schematic representation of the MMC [18], (b) the half-bridge, (c) the full-bridge, (d) the clamp-double, (e) the three-level FC, (f) the three-level NPC, and (g) the five-level cross-connected SM [34, 18].

2.3.2 Permanent magnet linear generator

Due to the availability of low-cost power electronic converters and the improvements of permanent magnet (PM) materials in terms of their remnant flux density, coercive force, and operating temperature, PM machines have been exploited in many applications. The permanents magnets (PMs) arrangement is used to have better flux linkage, reduce cogging force, and increase generation efficiency in WECs [16].

The current linear PM generators (LPMG) technologies can be classified according to different characteristics. The tubular shape of linear generators generates a high energy density, and the planar shape reduces detent force by its structure [4], [23], [51]. The tubular permanent magnet linear generator (TPMLG) has several topologies depending on the stator/translator relation, such as single/single, single/dual, or dual/single [61]. The configurations of PMs in linear machines are related to the flux direction, and they can be radial, axial, or Halbach array [45]. Also, there are topologies with a fixed and variable air gap length to avoid demagnetization [28].

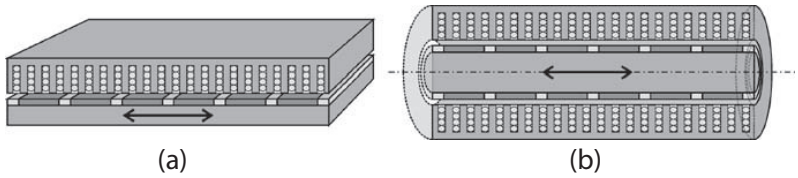

Figure 2.5: Types of Linear Generators: a) Flat, and b) tubular linear generator, images from "Ocean wave energy: current status and future perspective" [15].

The structure of a linear generator may be flat or tubular, as shown in Figure 2.5. Fabrication of the flat-type generator is easy, and it can be designed with a different number of sides, reducing the manufacturing cost, simplicity of installation, and bearings maintenance. Double-sided and multiple-sided structures are preferred to balance the attraction force between the stator and translator. If the tubular structure is used, the edge effects are eliminated due to the cylindrical geometry's closed form.

Because of the reciprocating linear motion, the stator or translator must be made longer to maintain the active operating system for a greater fraction of the stroke. The PM translator is usually longer than the stator, which means that the entire stator winding is active during the whole stroke, and at the same time, the amount of series copper and the conduction losses are reduced.

The translator can be placed inside or outside of the generator. In a 2 MW linear generator designed for the AWS system, the stator is in the middle of two translator sides, whereas the translator of the $10kW$ Uppsala University generator is placed in the middle of a four-sided stator. It has been found that the power density of the external tubular PM linear generator (ETPMLG) is 7–8 times higher than that of the internal one when the volumes of both configurations are the same.

The PMs are assembled on the translator in the above-mentioned linear generators, increasing the mover structure's complexity, thermal instability, and demagnetization risk. These problems have been solved by assembling the PMs and armature coils on the stator while the translator only contains iron.

The linear generators can be designed to be longitudinal or transverse flux. The installation of permanent magnets in longitudinal flux generators for direct-drive WECs has been designed to be radial, axial, Halbach, and quasi-Halbach. The stator coils lie transverse to the axial length in a transverse flux PM (LTFPM) machine. The LTFPM machine was developed as one of the preferred generators in applying WECs, because of its high efficiency at low speeds [49].

There are significant differences between the performance of iron-cored and air-cored structures. The induced voltage amplitude and the power output of the iron-cored linear generator are considerably higher than those of the air-cored one. The RMS voltages ratio is approximately equal to 3 [23]; it is reasonable since the magnetic flux inside the iron core is higher due to the low reluctance.

Furthermore, air-cored structures exhibit lower power density and efficiency than iron-cored counterparts. However, some disadvantages, such as low power factor, large magnetic attraction forces, structural, bearing, and lubrication requirements, are eliminated in the former.

3 MATHEMATICAL MODEL AND CONTROL STRATEGY

3.1 System Model of a Point Absorber

A WEC system typically uses three energy conversion stages to feed the grid. The point absorbers have the advantage of reducing the two first stages in a direct stage. This design uses the action of the incident sea waves to move the translator of a linear generator without additional mechanical systems [10]. This device has a buoy on the wave surface and is connected to an electrical generator system underwater, as shown in Figure 3.1. The last stage is the interface between the WECs and a common coupling point through a static transmission cable, and this provides a power signal to inject into the grid, as shown in Figure 3.1. The focus of this paper is on the direct stage.

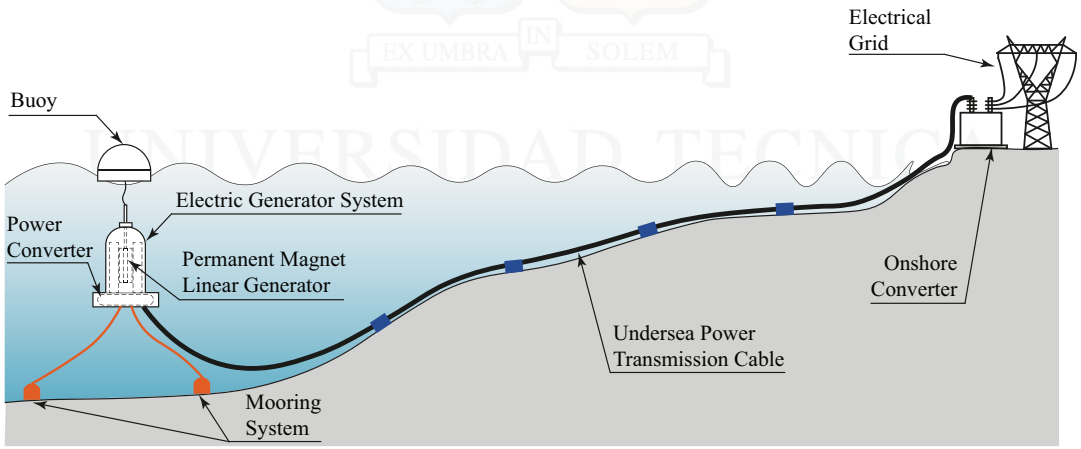

Figure 3.1: Complete system of a wave energy converter.

3.1.1 Wave-Buoy Interaction

The wave elevation defines the potential energy (E_p), and the water fluid motion defines the kinetic energy (E_k). These energies are stored in the waves, as shown in Equation 3.1 [25, 13]:

$$E = E_p + E_k = \rho g \int_0^\infty S(f)df = \frac{\rho g H_s^2}{16}\,, \tag{3.1}$$

where ρ is the fluid density (approximately 1025 $\frac{kg}{m^3}$), g refers to the gravitational acceleration (9.8 $\frac{m}{s^2}$), E

is total stored energy, and $S(f)$ is the spectrum distribution of the wave energy of a given location as a wave frequency function (f). The wave spectrum defines the average height (H_s), as shown in Equation 3.2; this is used to determine the wave power [25, 33].

$$\frac{H_s^2}{16} = \int_0^\infty S(f)df \ . \tag{3.2}$$

The integral of the time-average energy transport per unit time and unit area in the direction of wave propagation (the x direction) is called the water-power level J or wave-energy transport, and its expression is shown below in Equation 3.3 using $v_g = g/2\omega$ for irregular plane waves on deep water [25, 13].

$$J = \rho g \int_0^\infty S(f)v_g(f)df = \frac{\rho g^2 T_J H_s^2}{64\pi} \ . \tag{3.3}$$

where T_j is the energy period, for example, an irregular wave of a buoy located in Valparaíso, Chile, where the depth is 4515 m, with energy period $T_J = 10.3$ s and significant wave height $H_s = 2.3$ m, the energy transport is $J = 26.6$ kW/m.

3.1.2 WEC Equation of Motion

The modifications made to the Figure 3.2 involve adding annotations for the vertical reference motion of both the buoy and the translator showing the forces applied to each one. The total force acting on the system (buoy and PTO) can be analyzed decomposed as illustrated in Figure 3.2. Incident waves produce the excitation force F_e, and the radiation force F_r is produced by buoy oscillation. The buoyancy force has a part constant F_b when the buoy stands still on the water surface $z_b = 0$; this represents the weight of the buoy and translator, and it also has a variable part $F_h = \rho g S z_b$ related to the displacement of the buoy and the balanced position. There is a gravity force $M_b.g$ and a force line F_{line}. These forces are written in the frequency domain as shown in Equation 3.4.

$$-w^2.M_b.z_b(w) = F_e + F_b - F_r - F_h - F_{line} - M_b.g \ . \tag{3.4}$$

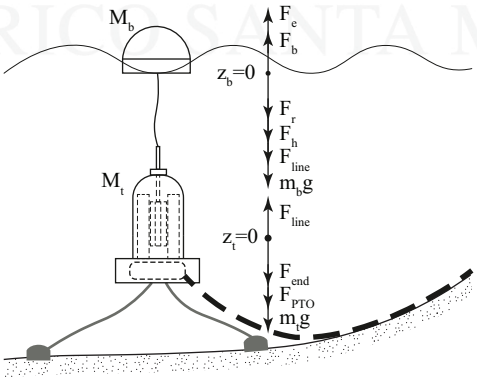

Figure 3.2: Characteristics of waves.

The force of the translator is the gravity force $M_t.g$, the line force is F_{line}, and the end-stop force is F_{end}. The latter force is generated when the translator hits the upper-end stop spring or the rubber damper hits the generator bottom. The F_{PTO} is the electromagnetic damping force from the power take-off.

$$-w^2.M_t.z_t(w) = F_{line} - F_{end} - F_{PTO} - M_t.g \ . \tag{3.5}$$

3.1.3 Power Take-Off

The PTO uses a linear generator with a tubular shape divided into two structures. The translator has ring-shaped PMs or PMs arrays with a similar shape, which have an axial configuration (north orientation to outer radial); furthermore, PMs arrays are attached to the PMs' support and a mobile vertical shaft, as shown in Figure 3.3. The stator has a tubular shape and supports five coils arranged around it.

The magnetic circuit can be analyzed using a lumped parameter method related to an electric circuit because they have the same behavior in a stable state [69]. The magnetic circuit is expressed in Equation 3.6, and it has a net reluctance ($\Re_{xx}$) given by the path of magnetic flux shown in Figure 3.3, the magnetomotive force ($\mathcal{F}_m$) produced by the PMs, and where Φ indicates the magnetic flux.

$$\mathcal{F}_m = \Phi \Re_n \ . \tag{3.6}$$

The reluctance ($\Re_{xx}$) is defined by the flux path length (l_x), vacuum permeability (μ_o), the relative permeability of each material (μ_{rx}), and the cross area (A_x), [37], as follows:

$$\Re_{xx} = \frac{l_x}{\mu_o \mu_{rx} A_x} \ . \tag{3.7}$$

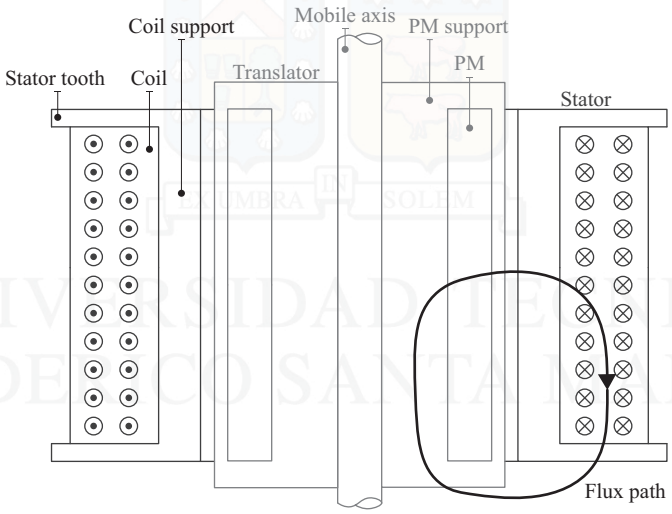

Figure 3.3: Schematic design of the linear generator. Figure based on [94].

The partial reluctance of the structure describes the net reluctance, using Kirchhoff's circuit laws [31], as shown below.

$$\begin{aligned} \Re_n = & \Re_{PM} + \Re_{oPMs} + \Re_{gap} + \Re_{cs} + \Re_c + \Re_l \\ & + \Re_{st} + \Re_{cs2} + \Re_{gap2} + \Re_{lPMs} + \Re_{iPMs} \ . \end{aligned} \tag{3.8}$$

Equation 3.9 defines the magnetomotive force ($\mathcal{F}_m$) generated by PMs. The magnetomotive force is the relation between the product of the remanent magnetization of the PM (B_r) with the width of the PM ($w_p m$) and the product of the relative permeability of the PM μ_{rpm} with the vacuum permeability (μ_o).

$$\mathcal{F}_m = \frac{B_r\, w_p m}{\mu_o \mu_{rpm}} \,. \tag{3.9}$$

The flux linkage is considered a sinusoidal function of the vertical displacement (z) to define the magnetic flux for each coil, as shown below.

$$\phi = \Phi_{max} \sin\left(\frac{\pi}{4\,\tau_m} z\right) = \frac{B_r\, w_m}{\mu_o \mu_{rm} \Re_n} \sin\left(\frac{\pi}{4\,\tau_m} z\right) \,. \tag{3.10}$$

Equation 3.10 is used to describe the electromotive force (ε) in a coil with many turns (N) [97]; thus,

$$\varepsilon = -N \frac{d\phi}{dh}\frac{dz}{dt} = -N \frac{B_r\, w_m}{\mu_o \mu_{rm} \Re_n} \frac{\pi}{4\,\tau_m} \cos\left(\frac{\pi}{4\tau_m} z\right) \frac{dz}{dt} \,. \tag{3.11}$$

3.2 Submodular Converter Description

An Full-Bridge and a Modular Multilevel DC Converter (DC-MMC) topology was used to harvest energy from each coil of the TPMLG to control the current harvesting process and generate a medium voltage for transmission. Therefore, each coil was connected to a power converter submodule, and the power converter submodule outputs were connected in series to generate a medium voltage, as shown in Figure 3.4.

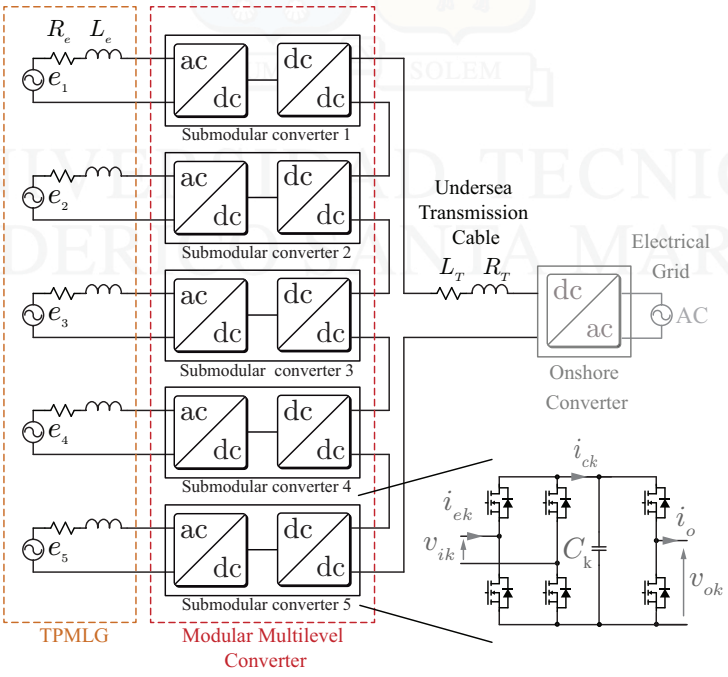

Figure 3.4: Modular inverter schematic with grid connections.

Each submodule comprised two parts interconnected with a coupled capacitor, as illustrated in Figure 3.4: an AC-DC converter from a generator coil and a DC-DC converter connected in series to other converters. In the first stage, a full-bridge submodule was used to control the current harvesting concerning the MPPT, which

changed the direction of the torque drive. The DC-MMC as second stage uses a half-bridge topology because two states were required to control the capacitor voltage. The DC-MMC connection could require a filter inductor if the transmission line inductance is insufficient to filter the switching harmonics.

We used a controlled decoupled design for the converters shown in Figure 3.5. The DC-MMC part used a half-bridge submodule to control the voltage of the capacitor.

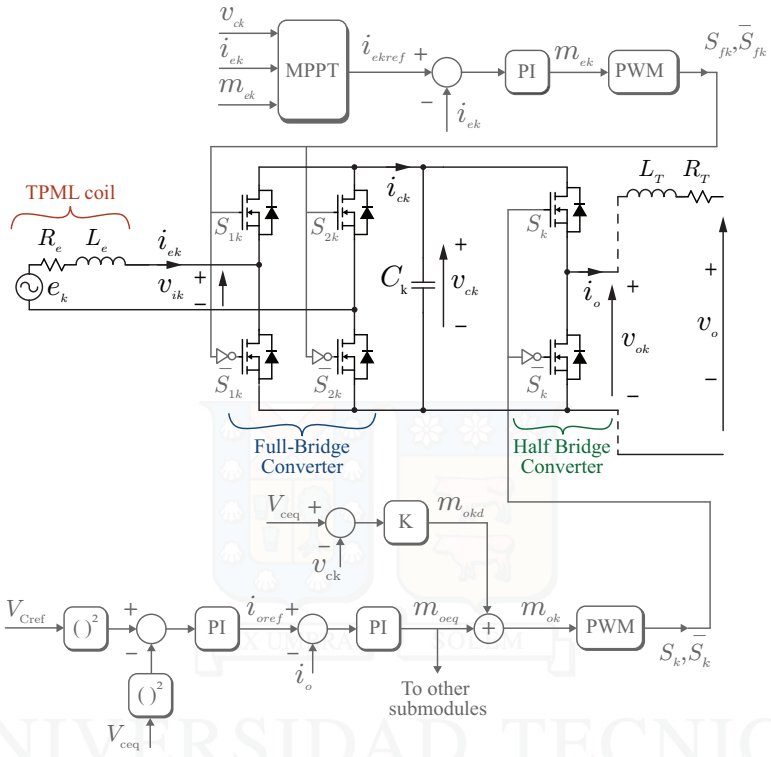

Figure 3.5: Control scheme and electronic circuit of an submodule.

One could add the submodules needed as coils have the generator through this configuration. At the same time, this decreases the frequencies generated by power.

Previous studies on PV systems have presented the same topology to interconnect low-voltage (PV) systems to medium- or high-voltage DC systems through one or two voltage transformer steps. These works show the viability of implementing this topology to large-scale connected grids [21].

3.3 Control Strategy

The proposed control strategy involves two decoupled control stages, one for an AC-DC converter with the MPPT and one for a DC-DC converter that assembles the DC-MMC, as shown in Figure 3.5. The first control stage uses the result of the MPPT method as a reference to control the harvesting current of a coil of the generator. The second control stage aims to control each DC-link voltage and the current through all the submodules of the DC-MMC.

3.3.1 Maximum Power Point Tracking (MPPT)

The MPPT method is essential to increase the efficiency of the wave energy converter by finding the optimal voltage and current of the generator proportional to the maximum output power. Due to its simplicity, the Perturb and Observe (P&O) method is commonly used as an MPPT technique, along with others such as dI/dV-Based, Neural Network Modeling, and Fuzzy Logic-Based Tracking. It involves adjusting a control variable with a fixed or variable step size to observe changes in the objective function until the power curve reaches zero slopes. The P&O method has the advantage of being relatively simple to implement, showing good tracking efficiency in slow changes, but its disadvantage is that it generates oscillations around the maximum power point (MPP), and the convergence time could vary. A flowchart explaining the MPPT control algorithm is presented in Figure 3.6. The iterative approach used in this method ensures efficient operation of the power converter with minimal oscillations, although some steady-state oscillations around the Maximum Power Point (MPP) region may persist.

The first part of the flowchart shows the voltage and current measurement of each coil, but these are filtered with a capacitor of $10\mu F$ to eliminate perturbations generated for switching.

The algorithm P&O method uses the converter duty cycle as a control variable. The duty ratio calculation is formulated as $D_n = D_{n-1} + \Delta D$, where D_n and D_{n-1} are the duty ratio for the current and previous time intervals, respectively. ΔD is the fixed step size. The P&O method operation principle is shown in Figure 3.6, where the power is evaluated in each time interval, and the duty ratio for the next cycle is obtained by adding or subtracting the fixed step size from the previous duty ratio, depending on the direction of the power change. MPPT methods based on fixed step size show good performance.

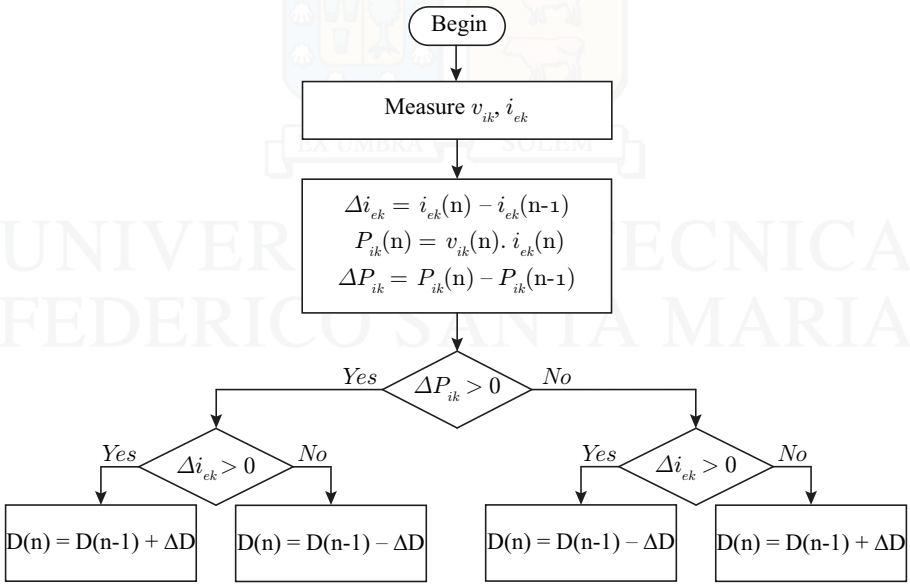

Figure 3.6: Flowchart for P&O (Perturb and Observe) MPPT control algorithm.

3.3.2 Full-Bridge Control

The MPPT algorithm determines the current reference for the AC-DC stage to maximize the power extracted from each coil. The proposed MPPT algorithm is based on the perturb and observes the electrical system measurements.

Considering a linear model of the windings, as shown in Figure 3.5, for a given harmonic ω_e, the input voltage can be calculated as:

$$v_{ik} = e_k - (R_e + j\omega_e L_e) i_{ek} \ . \tag{3.12}$$

The active power at the converter terminals can be calculated as follows:

$$P = \mathbb{R}\{v_{ik} i_{ek}^{*}\} \, . \tag{3.13}$$

Calculating from the previous equations, the current which generates the maximum active power results in

$$I_{ekd} = \frac{E_{kd}}{2R_e} \, , \tag{3.14}$$

$$I_{ekq} = \frac{E_{kq}}{2R_e} \, , \tag{3.15}$$

where $I_{ek} = I_{ekd} + jI_{ekq}$ and $E_k = E_{kd} + jE_{kq}$ are the direct and quadrature components of the input current and induced voltage phasors, respectively. From the previous result, it is possible to notice that to obtain the maximum active power, the current must be in-phase with the induced voltage. Repeating the previous analysis but solving for the converter voltage results in

$$V_{ikd} = \frac{E_{kd}}{2} - \frac{\omega_e L_e}{R_e} \frac{E_{kq}}{2} \, , \tag{3.16}$$

$$V_{ikq} = \frac{E_{kq}}{2} + \frac{\omega_e L_e}{R_e} \frac{E_{kd}}{2} \, , \tag{3.17}$$

where $V_{ik} = V_{ikd} + jV_{ikq}$ (components in coordinates dq) is the converter input voltage phasor. Therefore, the voltage at the converter terminals is a combination of the direct and quadrature component of the induced voltage at a given frequency.

It is impossible to directly obtain the voltage or current reference because the induced voltage cannot be measured. This paper employs a perturb-and-observe algorithm by measuring the current, capacitor voltage, and modulation index and generating a reference for the input current according to the calculated power; the values of L_t and R were considering that the transmission line should reach the on-shore converter. The values of L_e and R_e used were approximated from the data of a linear generator from Gieras [30].

$$\frac{i_{gk}}{m_k} = -\frac{v_{ck}}{R_e + sL_e} \, . \tag{3.18}$$

The model of the input current in terms of the modulation index in the domain of frequency "s" is

$$I_{ek}(s) = \frac{-V_{ck} M_{ek}(s)}{L_e s + R_e} \, , \tag{3.19}$$

where I_{ek} is the coil current, M_{ek} is the modulation index for the converter, V_{ck} is the capacitor voltage, R_e is the coil resistance, and L_e is coil inductance. Once the current reference is obtained, a PI controller generates the modulation index. This controller is designed by pole placement using the previous equation.

After the PI controller generates the modulation signal, a bipolar Pulse-width modulation (PWM) is employed to generate the switching signals for the full-bridge converter.

3.3.3 Half-Bridge Control

The main control objective of the half-bridge control scheme is to transfer the power from the DC-link to the output terminals and to keep the capacitor voltages balanced at a given level.

Each winding generates a different amount of power transferred from the input terminals to the output terminals of the submodule. The output current is the same for all submodules; hence the output voltage

must differ. Considering the capacitor voltages controlled at the same value, the modulation indexes for each submodule must also be different.

The control system consists of a mean component controller and a differential component controller to manage the power transferred in all the submodules. These are analyzed below.

The total output voltage is defined by

$$v_o = \sum_{k=1}^{N} v_{ok} = \sum_{k=1}^{N} v_{dck} m_{ok} \ . \tag{3.20}$$

Considering both the capacitor voltages and the modulation indexes, different in each submodule, this voltage can be written as

$$v_o = \sum_{k=1}^{N} (v_{dceq} + v_{dckd})(m_{oeq} + m_{okd}) \ , \tag{3.21}$$

where v_{dceq} and m_{oeq} are the mean values of the capacitor voltage and modulation index, respectively, and v_{dcd} and m_{okd} are the differential components of the capacitor voltage and modulation index, respectively. Defining the mean value as

$$v_{dceq} = \frac{1}{N} \sum_{k=1}^{N} v_{dck} \ , \qquad m_{oeq} = \frac{1}{N} \sum_{k=1}^{N} m_{ok} \ , \tag{3.22}$$

results in

$$\sum_{k=1}^{N} v_{dckd} = \sum_{k=1}^{N} m_{okd} = 0 \ . \tag{3.23}$$

Replacing the output voltage definition and neglecting the product of differentials results in

$$v_o = N v_{dceq} m_{oeq} + v_{dceq} \sum_{k=1}^{N} m_{okd} + m_{oeq} \sum_{k=1}^{N} v_{dckd} + \sum_{k=1}^{N} v_{dckd} m_{okd} = N v_{dceq} m_{oeq} \ . \tag{3.24}$$

Therefore the total output voltage, and hence the output current, is given by the mean value of the modulation index.

Considering an inductive-resistive load to model the transmission line, the onshore converter, and the electrical system, the dynamical equation is given by

$$L_T \frac{di_o}{dt} + R i_o = N v_{dceq} m_{oeq} \ . \tag{3.25}$$

The mean current PI controller is designed using the previous equation by the pole placement technique, adjusting a response time of 5 ms.

In each capacitor, the voltage is given by the following dynamical equation.

$$C \frac{dv_{dck}}{dt} = m_{ek} i_{ek} - m_{ok} i_o \ , \tag{3.26}$$

where i_o is the output current, m_{ok} is the modulation index for the half-bridge, m_{ek} and i_{ek} are the modulation index and current in the full-bridge, and C is the capacitance. The current coming from the full-bridge is considered a system disturbance, so it is neglected. Calculating the mean capacitor voltage results in

$$C\frac{dv_{dceq}}{dt} = -\sum_{k=1}^{N}(m_{oeq} + m_{okd})i_o = -m_{oeq}i_o \ . \tag{3.27}$$

Multiplying by the mean voltage to obtain the power and considering a constant line voltage V_L imposed by the onshore converter, the model results in

$$\frac{C}{2}\frac{dv_{dceq}^2}{dt} = -V_L i_o \ . \tag{3.28}$$

Therefore, to increase the energy in the capacitor (i.e., the square of the capacitor voltage), the output current must be reduced and vice versa. Using this dynamical model, a PI controller for the output current using the pole placement technique is designed to adjust the response time to 50 ms, this time is a decade slower than the response time of the current control because it is a cascade control system, and the current control needs time to stabilize the response to the reference given for the voltage control.

Once the output current is controlled, Equation 3.26 can be written in terms of the differential values as

$$C\frac{dv_{dckd}}{dt} = -m_{okd}i_o \ . \tag{3.29}$$

Considering this expression, the relation between the differential voltage capacitor and the differential modulation index is integral, and hence, a proportional term K can be used for control, as shown in Figure Figure 3.5.

The modulation index of each submodule composed of the mean and differential values is modulated using PWM to generate the gating signals for the half-bridge converter.

4 SIMULATION RESULTS

The thesis presents numerical simulation outcomes from time-domain simulations of dynamic systems, modeled using state-space equations with specific electrical component models. A concise overview of the numerical integration tools and simulation configuration is provided.

4.1 Simulation Software

A wide range of software packages are available that provide preprogrammed algorithms for numerical integration. This study solved the mathematical models by implementing them in PLECS, a software package specialized in electrical circuit simulation and analysis.

4.1.1 PLECS

PLECS, also known as Piecewise Linear Electrical Circuit Simulation, is a software program used primarily for simulating electrical circuits in the design and analysis of power and control systems. PLECS focuses explicitly on power systems, employing models based on state variables and electrical component models.

PLECS offers an intuitive graphical interface that enables users to construct and simulate electrical circuits. Users can easily drag and drop various electrical components within a visual design environment, such as power sources, resistors, inductors, capacitors, switches, converters, and more. Once the circuit is built, users can customize the characteristics and parameters of each component according to their requirements. Input stimuli, such as voltage or current signals, can be configured, and the system's initial conditions can be defined.

During real-time simulations within PLECS, the program calculates and presents voltage and current waveforms for each component and other relevant variables.

In addition to real-time simulation capabilities, PLECS provides various analysis and visualization tools that enable users to conduct detailed studies of system behavior. These tools include stability analysis, harmonic analysis, transient analysis, and frequency response analysis.

PLECS is a powerful electrical circuit simulation program with an intuitive graphical interface. It is specifically tailored for power and control systems and is widely used to design and evaluate complex electrical systems.

4.1.2 Add-on PLECS Coder

Typically, a code generator transforms an intermediate representation of source code into machine code. The PLECS Coder, an extension of PLECS Blockset and PLECS Standalone, performs this task. It generates ANSI-C code from a PLECS model, which can then be compiled for execution on the simulation host or a designated target. This target may include an embedded control platform or a real-time digital simulator. Furthermore, the PLECS Coder can generate embedded code tailored explicitly for particular hardware targets.

4.2 Simulation Description

PLECS allows the creation of a graphical program to control the converters to be implemented. This program can be loaded into the experimental controller. The simulation was divided into three blocks: two for control and one for the implemented setup, as shown in Figure 4.1. The first block, "Controller FB F28379D", has two functions: to generate control signals to produce waveforms that simulate a linear generator's behavior and to apply the full-bridge control described in the subsection 3.3.2. The second block, "Controller HB F283336", performs the half-bridge control described in the subsection 3.3.3.

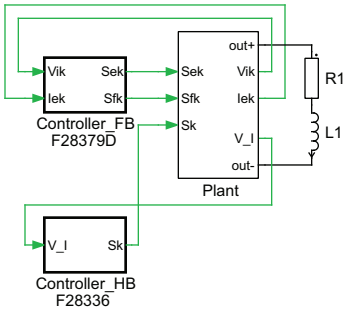

Figure 4.1: General Schematic of the simulation.

The block called "Plant" in Figure 4.1 is composed of three cells, each of which is divided into three parts: the first part of each cell is composed of a full-bridge that switches to simulate the behavior of the coil in a linear generator, for which a transformer and a resistor representing the electrical characteristics of a generator are used. The remaining part corresponds to the proposed MMC (Modular Multilevel Converter), which consists of a full-bridge and an output half-bridge connected by a DC-link capacitor, as explained in the previous section. Figure 4.2 shows the schematic of the implemented Plant block for simulating the behavior of a linear generator and the proposed MMC.

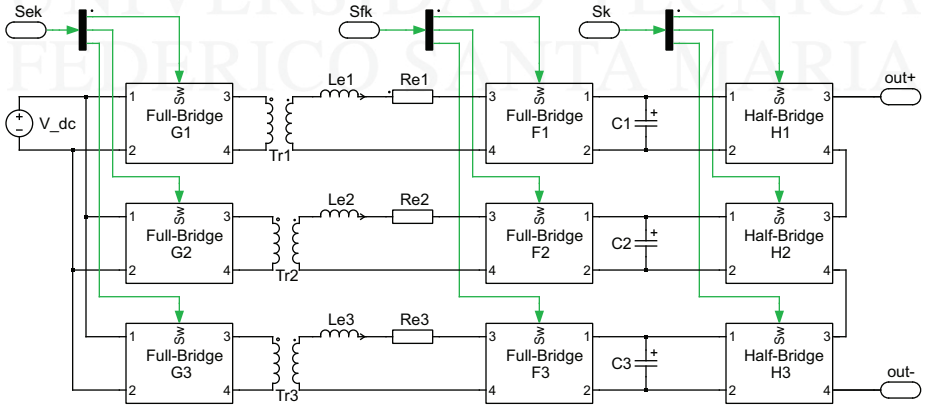

Figure 4.2: Schematic of the linear generator and the proposed MMC.

Table 4.1 shows the system parameters used in the simulation, where R_e and L_e represent the resistance and inductance of a coil in the linear generator, C denotes the capacitance of the DC-link, and L_T and R are the equivalent transmission inductance and resistance, respectively, from Figure 4.1.

The simulation will be executed over a time period of 4 seconds to verify the behavior of the proposed converter. During the initial 2 seconds, the proposed controllers will be applied, and in the remaining time, the

capacitor voltage balancing will be activated to observe its performance. The label "I" indicates the start of the capacitor voltage balancing operation.

Table 4.1: Parameters of the WEC system.

Parameter	Value
Coil Inductance (L_e)	15 mH
Coil Resistance (R_e)	1 Ω
DC capacitance (C)	2.200 μF
Line Inductance (L_T)	20 mH
Equivalent system resistance (R)	10 Ω

4.3 Results Analysis

The simulation is scaled to wave periods of 1[Hz] to accelerate the simulation time, which does not affect the behavior of the proposed system. Figure 4.3 shows the simulated voltage of a TPMLG with three coils to show its behavior, which to explain in the section before using a voltage source (V_{dc}), a transformer (Tr_x), and passive (R_e and L_e) elements. In order to obtain a peak induced voltage of 40[V], a voltage source of 6[V] was set up to pass through a full-bridge, producing a switched voltage that emulates the behavior of the induced voltage. Subsequently, this voltage is increased and isolated using a transformer to replicate the induced voltage of a linear generator. Figure 4.3.b shows the voltage at the secondary side of the transformer filtered, demonstrating that the mean voltage perfectly simulates the behavior of an induced voltage from a TPMLG.

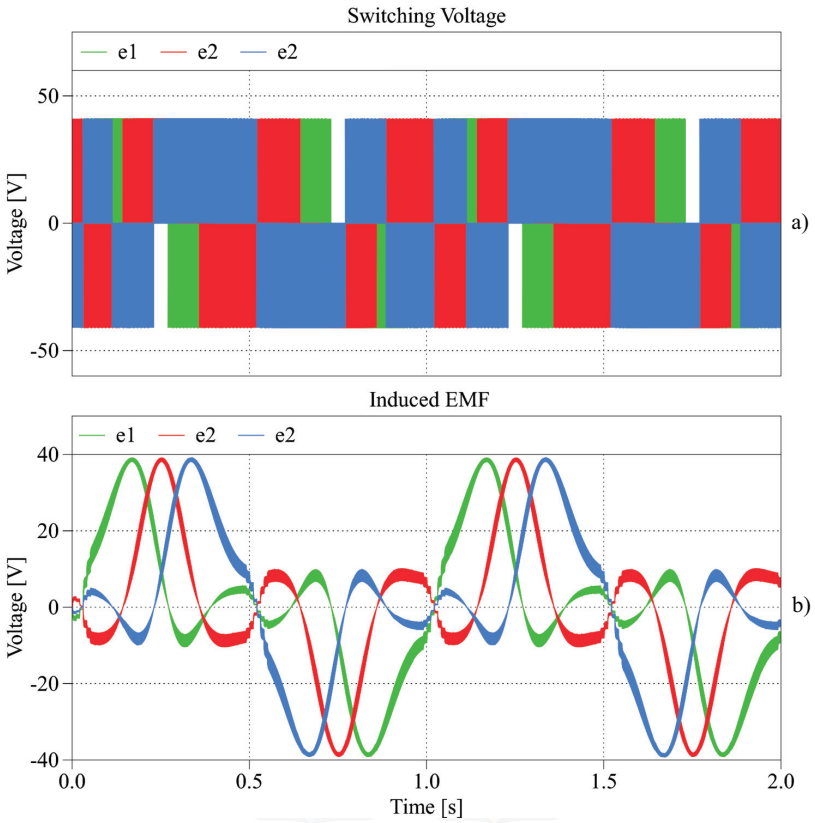

Figure 4.3: Voltage generated at the terminals of the coils (secondary of the transformer). a) Voltage measurement in terminals, b) Voltage filtered.

Figure 4.4 shows the Voltage and current signal in the input of the first stage of the converter, the behavior change after the mark "I", the current is more stable after the mark. The MPPT is used to harvest energy in this stage and charge the DC-link capacitors.

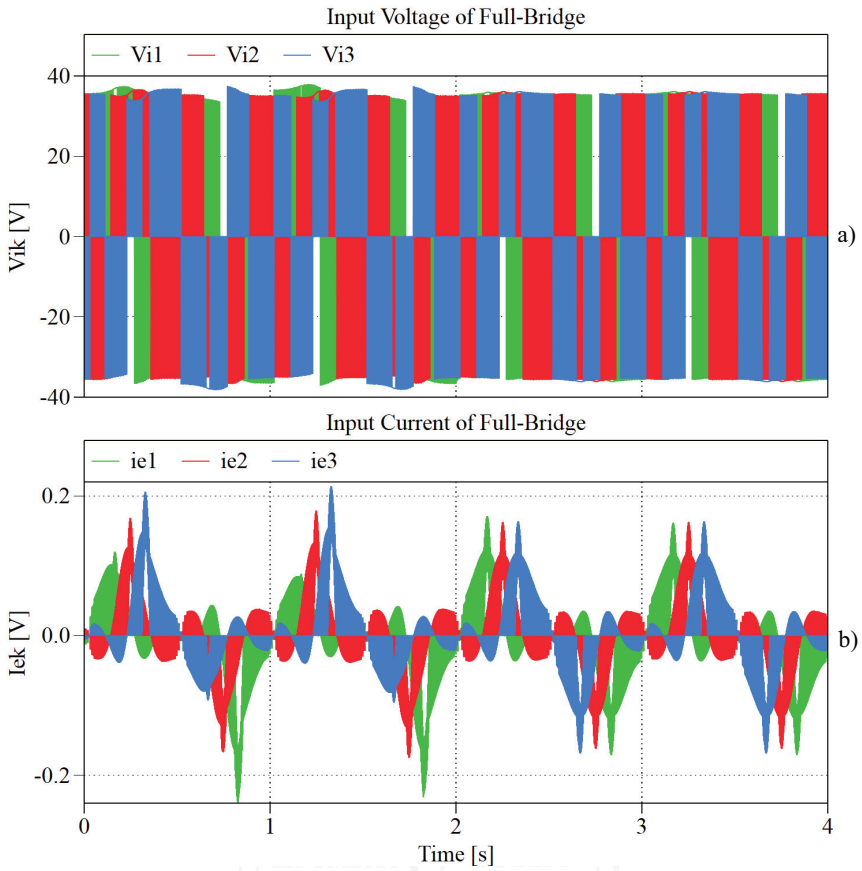

Figure 4.4: (**a**) Measured voltage in the input of the each submodule v_{ik}. (**b**) Input current harvesting $i_e k$.

Figure 4.5 illustrates the behavior of the DC-Link capacitor voltage. In the initial stage, it can be observed that the capacitors are consistently charging and discharging. In the subsequent stage, the voltage stabilizes around 30[V]. The control of the final stage also varies with the three capacitors to keep their voltage constant.

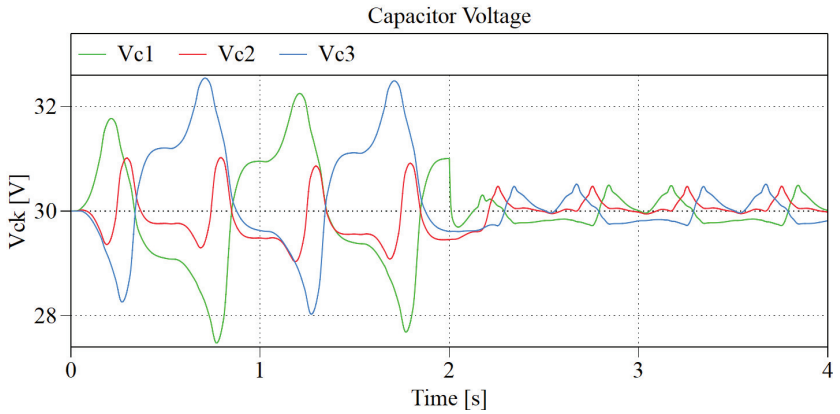

Figure 4.5: Capacitor Voltage V_{ck} in each submodule

Figure 4.6 shows the output voltage and the modulation index of each submodule, the signal of the PI regulator changes between 0 – 1, and the behavior between the three submodules changes to maintain the voltage constant.

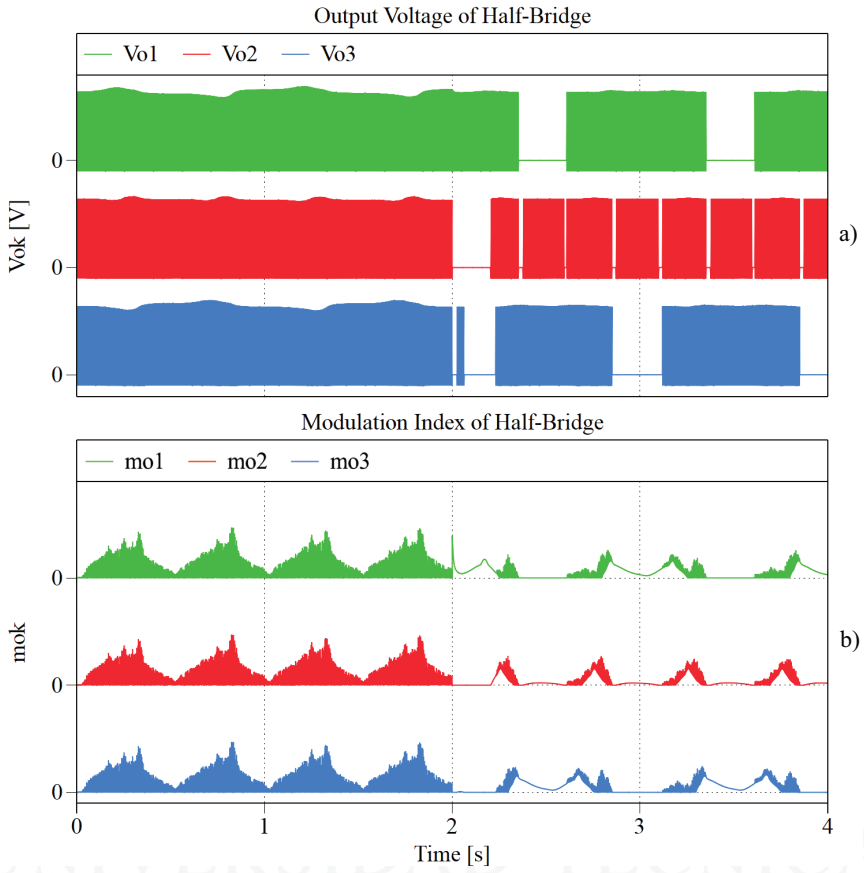

Figure 4.6: (**a**) Measured output voltage V_{ok} in each submodule. (**b**) Modulation index m_{ok}.

Figure 4.7 displays the output current of the converter, which flows through the series-connected submodules and an RL load with values provided in Table 4.1. The output current becomes more stable after the load balancing of the capacitors is activated.

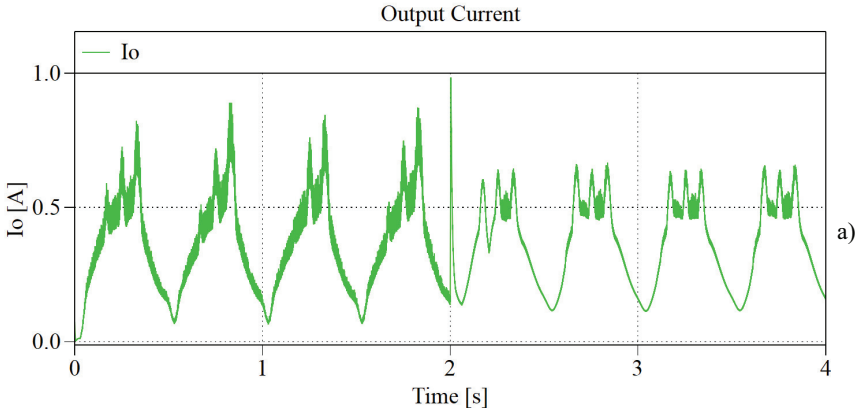

Figure 4.7: Output Current i_o general.

4.3.1 Analysis of Efficiency

In order to obtain the experimental efficiency, SiCFet G3R75MT12D is used to add losses in the simulation, the power is calculated using sampled values of voltage and current (neglecting the high frequency of commutation). Measurements are taken from the inputs of each sub-module and the resulting powers are summed to obtain power harvesting. Output power is defined as a measurement of the voltage and output current of each submodule. These measurements are made with and without capacitor voltage balance. Efficiency μ is defined as the relation between the output and harvesting power, as shown in Equation 4.1.

$$\mu = \frac{P_o}{\sum_{k=1}^{N} P_{ik}} = \frac{\sum_{k=1}^{N} v_{ok} * i_o}{\sum_{k=1}^{N} v_{ik} * i_{ek}} \,. \tag{4.1}$$

According to previous research [9], utilizing coils connected in series in a linear generator yields an efficiency of 98%. The proposed converter exhibits an average efficiency of 83.6% in the initial stage when employing the designed controllers. Subsequently, the efficiency increases to 83.7% due to capacitor voltage balancing. The measurements of this calculus are made with the converter in a stable state.

4.4 Farm of Wave Energy Converters

The development of Wave Energy Converters (WECs) addresses the significant reliance on fossil fuels, particularly in areas where grid connection remains uncertain. The PTO absorbs the wave energy directly by the generator translator, dispensing with the mechanical interface and offering higher efficiency and fewer repairs and costs [38]. However, the voltage and power profiles are proportional to the wave movement, requiring special machine drives and a converter to be connected to the grid. Wave oscillations have low frequency and high forces [27]. These oscillations are a disadvantage when the translator reaches the ends of the linear generator at positions 1 and 9, as shown in Figure 4.8.

Power oscillations can be reduced in several ways: one approach uses a battery bank system with a certain degree of complexity, and another is the implementation of WECs farms. If the power demand is high, multiple WECs can be used, as shown in Figure 4.9.

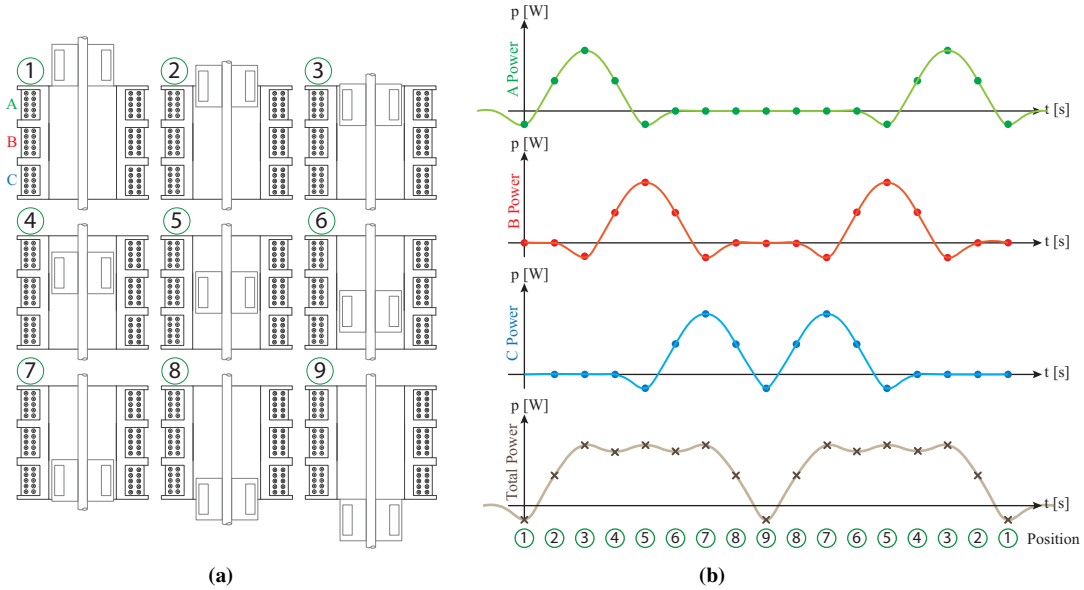

Figure 4.8: Power oscillation analysis: (a) Position of translator (b) Behavoir of power

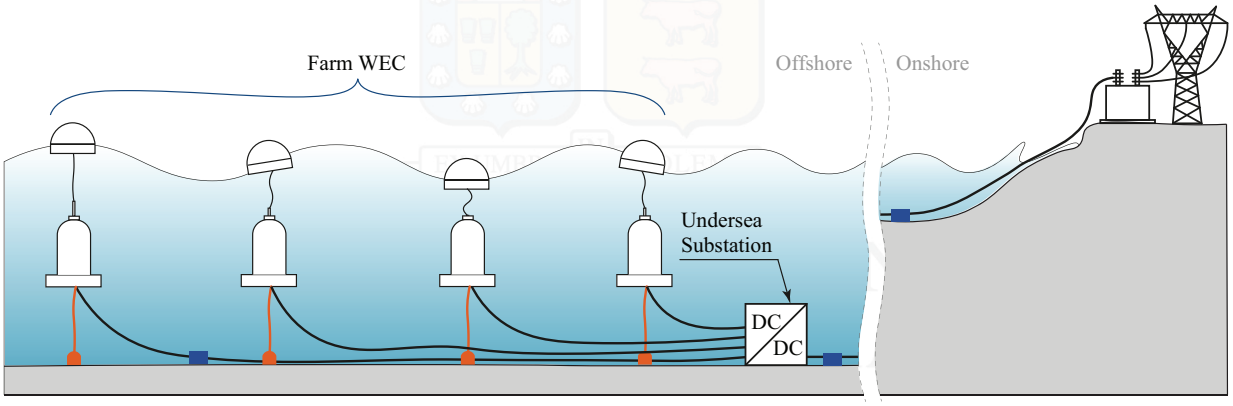

Figure 4.9: WECs farm.

The position of the WECs is crucial in a farm; they should be arranged geometrically to compensate for the mentioned oscillations. In Figure 4.10, it is shown that the resulting power from the buoys can compensate for the oscillations and produce a more stable power output. This solution is mentioned as it will be further explored in future research.

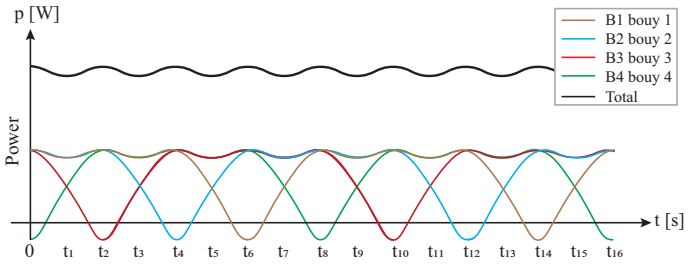

Figure 4.10: Behavior of the power outputs of a WEC farm.

5 | EXPERIMENTAL VALIDATION

The experimental validation was conducted based on a power hardware-in-the-loop (PHIL) system with modifications. PHIL serves as a natural extension of Hardware-in-the-Loop (HIL), enabling real-time simulation environments to transmit the required rated power. PHIL simulation provides a platform by incorporating the entire complexity of the controlled plant into the embedded system. This is achieved by employing mathematical models of all dynamic systems related to the controlled plant, forming what is known as the 'plant simulation.' The embedded system being tested interacts with this plant simulation.

In this particular case, the Delfino controller manages the generation of voltage as a TPMLG. It is electrically connected to the DC-MMC proposed to be controlled with other Delfino controllers, and the output of the converter is connected to a load RL. Consequently, the physical plants were implemented, and only the controls were software-implemented. The PC was exclusively used to monitor the desired variables and to load programs onto the controllers, as illustrated in Figure 5.1.

The setup was created using two development boards, executing the program implemented in PLECS. They are essential for simulating the behavior and system control of linear generators. The simulation of the linear generator behavior is implemented using a full bridge, which generates multilevel signals; in addition, transformers are used to isolate the stages, filter the signals and obtain the necessary resistance and inductance. The topology of the converter implemented is developed into three windings; each winding is connected to a full-bridge, which is linked to a DC-link capacitor, and then is connected to a half-bridge, as described in the previous section.

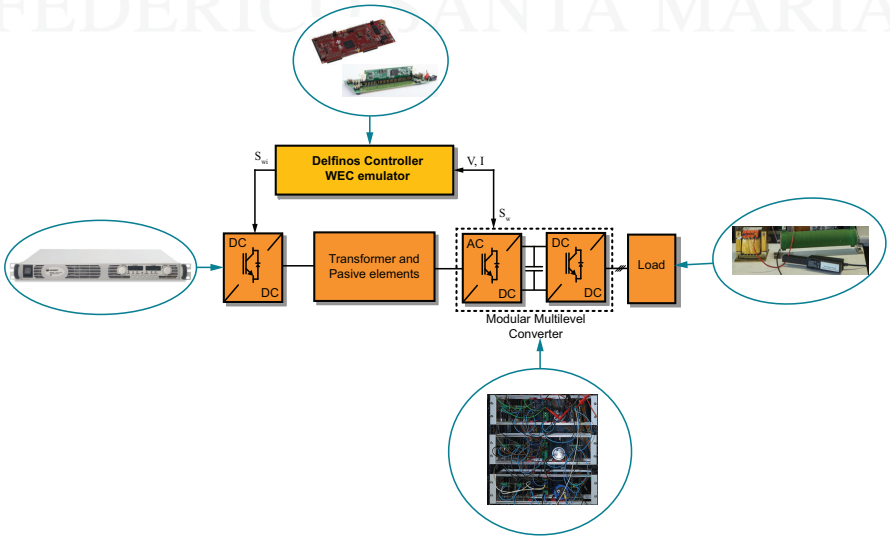

Figure 5.1: Schematic of the setup implemented.

5.1 Development board

The HIL simulation was conducted using two development boards. The first board is responsible for simulating the behavior of a linear generator and controlling the first full-bridge. The second board is dedicated solely to the half-bridge control. Below are the main features of the development boards.

Controller F283336: The "Controller F283336" is a powerful microcontroller designed for complex control and signal processing applications. It features a 32-bit C28x CPU, which provides fast and efficient execution of control algorithms. With a clock frequency of 100 MHz, it offers real-time processing capabilities, making it suitable for time-critical tasks.

Equipped with 256 KB of Flash memory and 68 KB of RAM, the "Controller F283336" provides sufficient space for program storage and data processing. It has various peripherals, including PWM, ADC, UART, SPI, and I2C, enabling seamless integration with external sensors, actuators, and communication devices.

The microcontroller's versatility and robust features make it well-suited for various applications, such as motor control, power electronics, inverters, and renewable energy systems. It is commonly used in industrial automation, automotive control, and other real-time control applications.

Controller F28379D: The "Controller F28379D" is a high-performance microcontroller tailored for advanced control and signal processing tasks. It boasts a 32-bit ARM Cortex-M4 CPU, delivering fast and efficient execution of complex algorithms. With a clock frequency of 200 MHz, it provides real-time processing capabilities, making it suitable for demanding real-time control applications. With 1 MB of Flash memory and 256 KB of RAM, the "Controller F28379D" offers ample memory for program storage and data manipulation. It includes various peripherals, such as PWM, ADC, UART, SPI, and I2C, facilitating seamless integration with external devices and sensors.

The "Controller F28379D" is highly versatile and finds application in various fields, including motor control, power electronics, robotics, and renewable energy systems. Its high-performance features make it an ideal choice for projects that require precise and efficient control in both industrial and automotive domains.

Both microcontrollers, "Controller F283336" and "Controller F28379D," offer powerful processing capabilities, extensive memory, and a wide range of peripherals, making them valuable choices for control-intensive applications in diverse industries. Table 5.1 shows the main features of this development board.

Table 5.1: Main Features of Development Boards

Feature	Controller FB F28379D	Controller F283336
Microcontroller	TMS320F28379D	TMS320F283336
CPU	32-bit ARM Cortex-M4	32-bit C28x
Clock Frequency	200 MHz	100 MHz
Flash Memory	1 MB	256 KB
RAM Memory	256 KB	68 KB
Peripherals	PWM, ADC, UART, SPI, I2C	PWM, ADC, UART, SPI
Communication	USB, CAN, Ethernet	UART, SPI, I2C
Applications	Motor Control, Power Electronics, Automotive, etc.	Motor Control, Inverters, Renewable Energy Systems, etc.

5.2 Experimental Results

An experimental setup is built to verify the proposed control scheme. The setup is shown in Figure 5.2, where it is possible to identify the submodules of the cascaded converter. The experimental setup comprises three submodules, each connected to the secondary of a transformer whose input signal emulates the induced

electromotive force (EMF) obtained in [96]. The output of the submodules is connected in series to an inductance and a resistance which model the underwater transmission line. Although the proposed cascaded multilevel converter is intended to generate medium voltage by using ten cells of $500V$ each, the experimental setup is limited to three cells due to the limited availability of converters to emulate the linear generator. The DC voltage of each cell is also reduced to $35V$ for safety purposes.

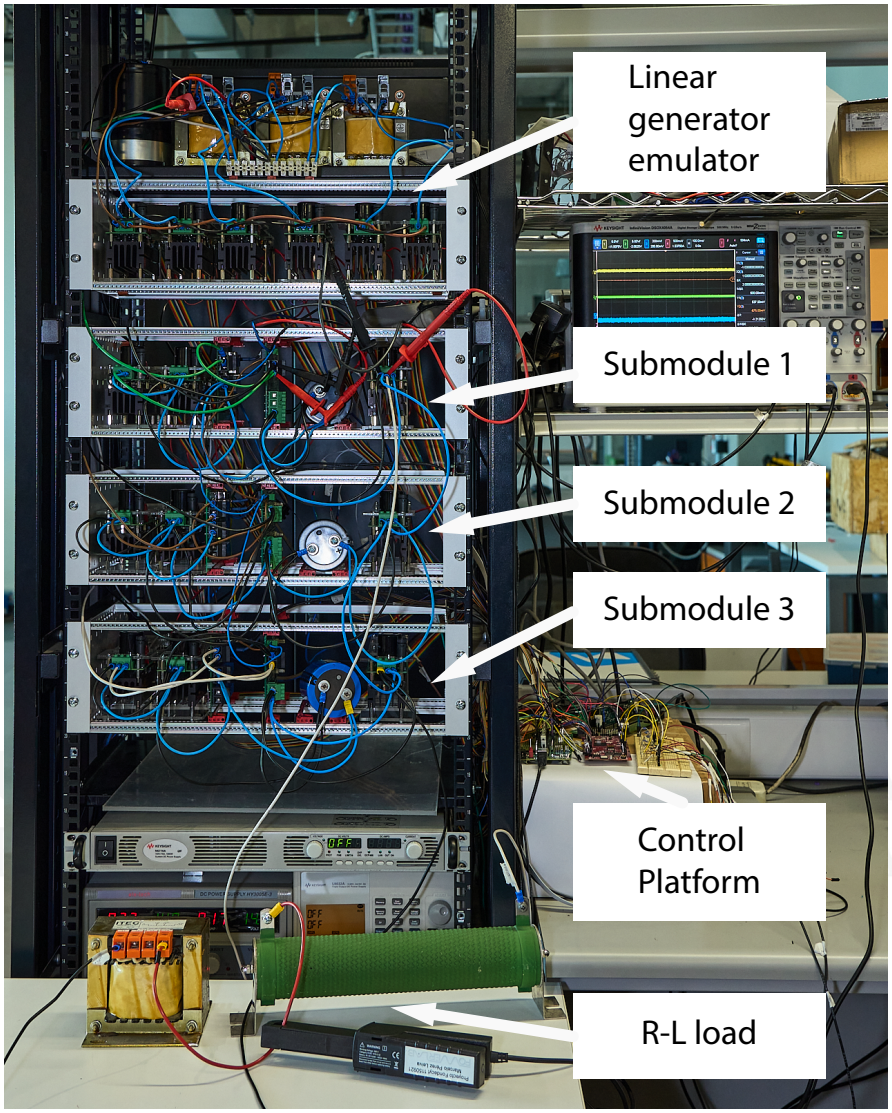

Figure 5.2: Picture of the experimental setup.

The control platform is based on two Texas Instruments (TI) Delfino boards. One board is used to control the linear generator emulator, and another board is employed to control the three submodules. The following results show the behavior of each submodule identified by the yellow, green, and blue colors, corresponding to submodules 1, 2, and 3, respectively.

Figure 5.3a shows the EMF voltages obtained from the linear generator emulator. The wave frequency was set to 1 Hz, and the height of the coils was defined as equal to the height of PMs. The translator is set to move between the first and the third coil; hence, no blank times without any induced voltage are generated.

Figure 5.3b shows the current extracted from the coils. The MPPT algorithm generates the reference of

this current. It is possible to notice that the current waveform resembles the induced EMF, as the analysis has shown.

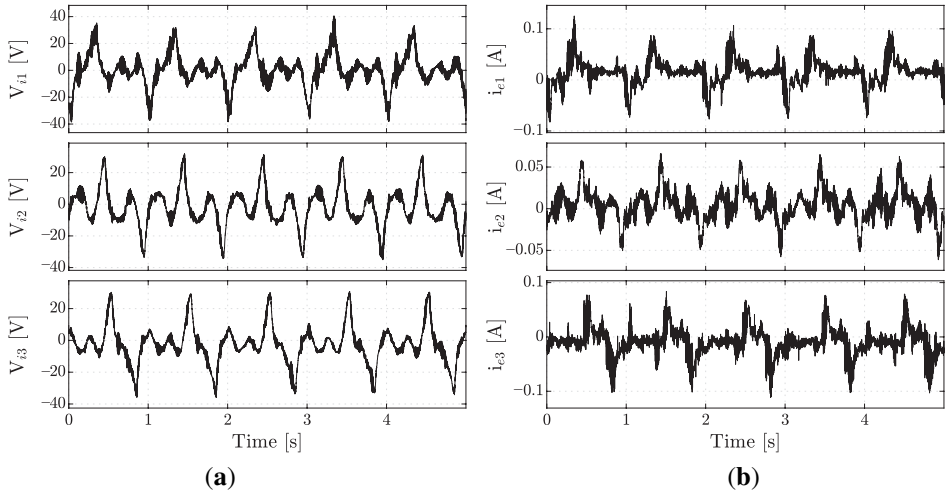

Figure 5.3: Experimental results. (**a**) Induced EMF. (**b**) Input submodule current.

Figure 5.4a shows the current flowing from the full-bridge converter to the capacitor. This current, as the capacitor voltage can be considered constant, resembles the power extracted from the coils of the linear generator.

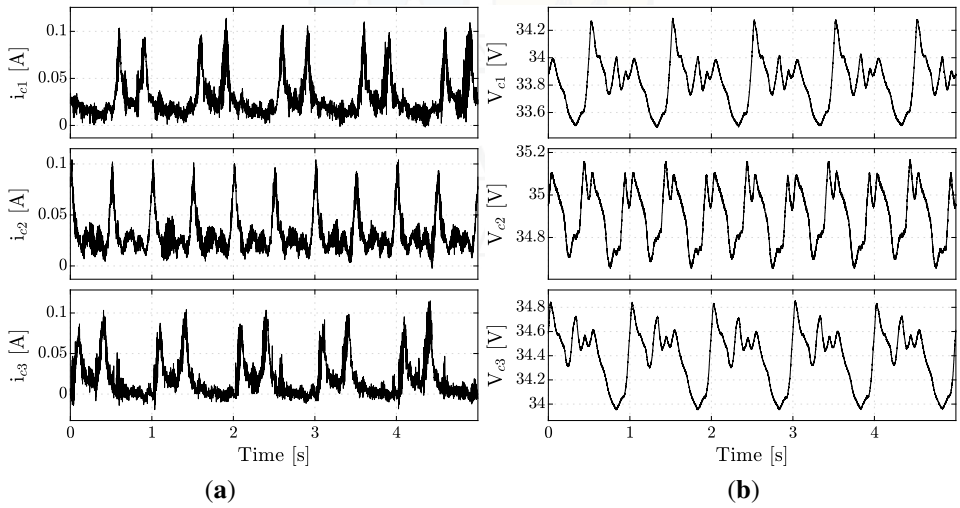

Figure 5.4: Experimental results. (**a**) Current flowing from the full-bridge to the capacitor (**b**) DC-link capacitor voltages.

Figure 5.4b shows the capacitor voltages. The mean value is set to $30V$, and the difference between them is less than $1V$.

Figure 5.5a shows the output current in pink color. This current combines the power injected by the three modules; hence, it resembles the total power extracted from the linear generator.

Figure 5.5b shows the activation of the voltage balancing loop. It is possible to notice that the voltages of the three capacitors are separated first, and they are balanced when the balancing loop is activated. There is a commercial model of WEC with an output voltage of 24 to $300V$ and a peak load power of $3kW$; our results have been designed to have an output voltage of $35V$ and a peak current of $200mA$.

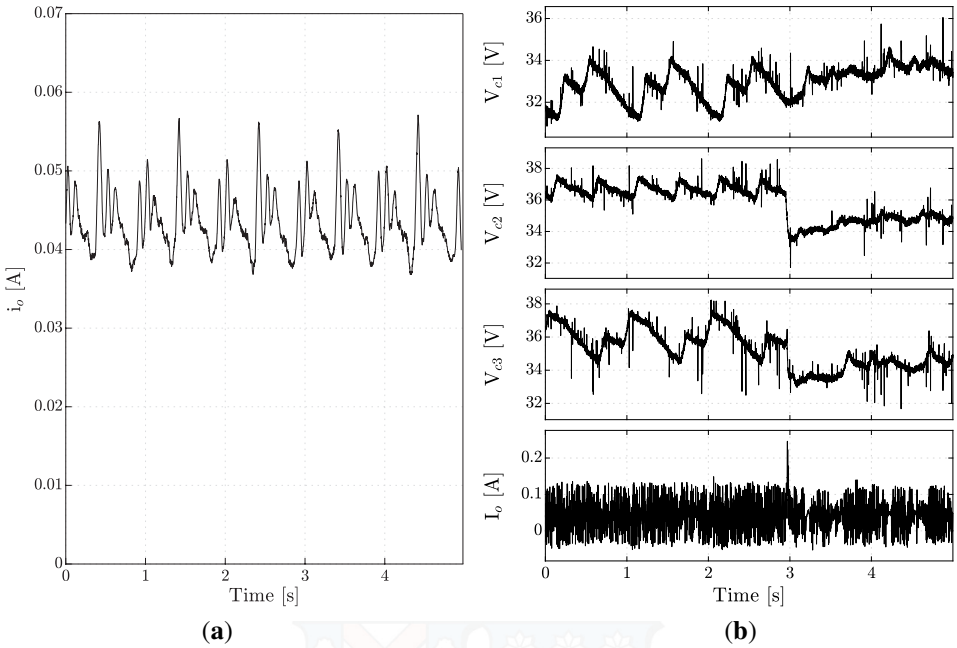

Figure 5.5: Experimental results. (**a**) Output current; (**b**) Performance of the capacitor balance strategy.

The power generated by direct conversion WECs, such as the one proposed in this paper, varies greatly due to the speed reduction at the top and bottom of the linear generator. The DC-link currents show this effect in Figure 5.4. However, it can be minimized by adding storage in the on-shore converter [73]. This converter is out of the scope of this paper.

5.2.1 Discussion of the results

To obtain experimental results, a regular wave motion with a period of $1[s]$ was assumed. This generates a signal resembling a *sinc* function, demonstrating that it induces maximum voltage when a coil aligns with a permanent magnet. At extreme positions, as the motion reverses due to changing direction, small reverse voltages are generated. The behavior of the induced voltage signal can be observed in the Figure 4.3.b of the simulation and Figure 5.3.a of this section. Both behave in the same manner, as the same procedure is employed to achieve this.

The experiments were divided into two behaviors, the first behavior refers to the normal operation of the controllers, and the other refers to the situation generated when capacitor voltage balancing is added to the control in the second stage. In Figure 4.4.b the current entering the first stage of the MMC is shown, where it can be observed that the harvesting current is more stable. Additionally, the behavior of the MPPT is generating a reference that allows charging the capacitors to a defined voltage with the balancing.

In Figure 4.5 and Figure 5.5.b, it is shown more clearly how the voltage balancing of the capacitors affects the system behavior, primarily in the simulation result. Starting from the second 2, the capacitor voltages begin to align to settle at $30V$, and the variations decrease drastically.

Using the Equation 4.1 defined for converter efficiency and applying it to the experimental part, an efficiency of 95% is obtained without voltage balancing, and 97% with capacitor balancing. This result is lower than the one obtained in the simulation, but it exhibits the same behavior.

6 | CONCLUSIONS AND FUTURE WORK

6.1 Conclusion

State of art of wave energy explain that it is an under-exploited resource with great potential and direct absorber WEC with linear generators present better results because they do not have mechanical connections; they also have the advantage of being placed offshore, avoiding visual contamination and problems with inhabitants near the coast.

This thesis shows a WEC system that uses a buoy as a point absorber and a linear generator as a PTO device. The linear generator has independent coils, which are powered sequentially as the shuttle rises and falls. A cascade converter drives the linear generator by connecting each coil to its respective converter submodule. The output of the submodules is connected in series to generate an average voltage to the transmission line. In the previous chapters, a mathematical analysis of the above-described system has been carried out to validate its behavior with its respective simulations and experimental results.

In this study, we proposed to improve the energy harvesting performance of WECs using a modular multilevel converter to drive a linear generator with independent coils by controlling the magnetic flux and torque depending on the translator position and increasing the efficiency of power transmission. The connection of the windings in series can be undertaken to generate a higher voltage and increase power transmission efficiency to the coast. The results demonstrate an efficiency of the proposed converter at 83.7%, calculated based on the power generated at the terminals of the coils of the linear generator. The load, representing the transmission line, is considered in this calculation. This efficiency is then compared with calculations presented in a similar paper.

The proposed control scheme is based on two stages: an MPPT algorithm to extract the power from the linear generator and transfer it to the DC capacitor and a DC capacitor controller to transfer the power from the capacitor to the transmission line. Experimental results show the controller performance, which allows for optimization of the energy extracted, balancing capacitor voltages, and power injection to the system.

6.2 Future Work

MPPT methods based on fixed step size show good performance, but their main drawbacks are the time to reach the maximum power point and the oscillations around the MPP. There is a trade-off between using large and small step sizes, as larger step sizes result in faster convergence but excessive steady-state oscillations, whereas smaller step sizes lead to slower response but reduced oscillations. [62].

Bibliography

[1] European Commission (EC). *Study on Lessons for Ocean Energy Development*. Tech. rep. Brussels: European Commission (EC), 2017, p. 62.

[2] European Marine Energy Centre Ltd. (EMEC). *Wave devices*. Mar. 2019. URL: http://www.emec.org.uk/marine-energy/wave-devices/.

[3] Ocean Energy Systems (OES). *System Web GIS, (accessed on March 2023)*. URL: https://www.ocean-energy-systems.org/ocean-energy/gis-map-tool/.

[4] Aamir Hussain Memon, T. b. Ibrahim, and N. Perumal. "Portable and pico-scale linear generator for wave energy conversion". In: *2014 5th International Conference on Intelligent and Advanced Systems (ICIAS)*. 2014, pp. 1–4.

[5] Izzeldin Idris Abdalla, Taib Ibrahim, and Nursyarizal Mohd Nor. "Analysis of Tubular Linear Motors for Different Shapes of Magnets". In: *IEEE Access* 6 (2018), pp. 10297–10310. DOI: 10.1109/ACCESS.2017.2775863.

[6] Tunde Aderinto and Hua Li. "Review on Power Performance and Efficiency of Wave Energy Converters". In: *Energies* 12.22 (2019). ISSN: 1996-1073. DOI: 10.3390/en12224329. URL: https://www.mdpi.com/1996-1073/12/22/4329.

[7] H. Akagi. "New trends in medium-voltage power converters and motor drives". In: *2011 IEEE International Symposium on Industrial Electronics*. 2011, pp. 5–14. DOI: 10.1109/ISIE.2011.5984128.

[8] E. Anderlini et al. "Control of a Realistic Wave Energy Converter Model Using Least-Squares Policy Iteration". In: *IEEE Transactions on Sustainable Energy* 8.4 (Oct. 2017), pp. 1618–1628.

[9] Aurélien Babarit. "A database of capture width ratio of wave energy converters". In: *Renewable Energy* 80 (2015), pp. 610–628.

[10] P. C. Binh et al. "Analysis, design and experiment investigation of a novel wave energy converter". In: *IET Generation, Transmission Distribution* 10.2 (2016), pp. 460–469.

[11] Markos I. Bonovas and Ioannis S. Anagnostopoulos. "Modelling of operation and optimum design of a wave power take-off system with energy storage". In: *Renewable Energy* 147 (2020), pp. 502–514.

[12] B. C. Boren et al. "Design, Development, and Testing of a Scaled Vertical Axis Pendulum Wave Energy Converter". In: *IEEE Transactions on Sustainable Energy* 8.1 (Jan. 2017), pp. 155–163.

[13] John Brooke. *Wave energy conversion*. Vol. 6. Elsevier, 2003.

[14] J. Cordonnier et al. "SEAREV: Case study of the development of a wave energy converter". In: *Renewable Energy* 80 (2015), pp. 40–52.

[15] Joao Cruz. *Ocean wave energy: current status and future prespectives*. Springer Science & Business Media, 2007.

[16] M. Curcic, J. E. Quaicoe, and R. Bachmayer. "A novel double-sided linear generator for wave energy conversion". In: *OCEANS 2015 - Genova*. 2015, pp. 1–7.

[17] B. Czech and P. Bauer. “Wave Energy Converter Concepts : Design Challenges and Classification”. In: *IEEE Industrial Electronics Magazine* 6.2 (June 2012), pp. 4–16.

[18] S. Debnath et al. “Operation, Control, and Applications of the Modular Multilevel Converter: A Review”. In: *IEEE Transactions on Power Electronics* 30.1 (2015), pp. 37–53. DOI: 10.1109/TPEL.2014.2309937.

[19] N. Delmonte et al. “Review of Oscillating Water Column Converters”. In: *IEEE Transactions on Industry Applications* 52.2 (Mar. 2016), pp. 1698–1710.

[20] Benjamin Drew, Andrew R Plummer, and M Necip Sahinkaya. *A review of wave energy converter technology*. 2009.

[21] J. Echeverría et al. “Multi-modular cascaded DC-DC converter for HVDC grid connection of large-scale photovoltaic power systems”. In: *IECON 2013 - 39th Annual Conference of the IEEE Industrial Electronics Society*. 2013, pp. 6999–7005. DOI: 10.1109/IECON.2013.6700293.

[22] Ottmar Edenhofer et al. *Renewable energy sources and climate change mitigation: Special report of the intergovernmental panel on climate change*. Cambridge University Press, 2011.

[23] J. Faiz and A. Nematsaberi. “Linear electrical generator topologies for direct-drive marine wave energy conversion- an overview”. In: *IET Renewable Power Generation* 11.9 (2017), pp. 1163–1176.

[24] António F.O. Falcão and João C.C. Henriques. “Oscillating-water-column wave energy converters and air turbines: A review”. In: *Renewable Energy* 85 (2016), pp. 1391–1424.

[25] Johannes Falnes and Adi Kurniawan. *Ocean waves and oscillating systems: linear interactions including wave-energy extraction*. Vol. 8. Cambridge university press, 2020.

[26] Fang Zheng Peng. “A generalized multilevel inverter topology with self voltage balancing”. In: *IEEE Transactions on Industry Applications* 37.2 (2001), pp. 611–618. DOI: 10.1109/28.913728.

[27] O. Farrok et al. “Design and Analysis of a Novel Lightweight Translator Permanent Magnet Linear Generator for Oceanic Wave Energy Conversion”. In: *IEEE Transactions on Magnetics* 53.11 (Nov. 2017), pp. 1–4.

[28] O. Farrok et al. “Oceanic Wave Energy Conversion by a Novel Permanent Magnet Linear Generator Capable of Preventing Demagnetization”. In: *IEEE Transactions on Industry Applications* 54.6 (Nov. 2018), pp. 6005–6014.

[29] F. Fusco and J. V. Ringwood. “A Simple and Effective Real-Time Controller for Wave Energy Converters”. In: *IEEE Transactions on Sustainable Energy* 4.1 (Jan. 2013), pp. 21–30.

[30] Jacek F Gieras, Zbigniew J Piech, and Bronislaw Tomczuk. *Linear synchronous motors: transportation and automation systems*. CRC press, 2016.

[31] Jacek F. Gieras, Zbigniew J. Piech, and Bronislaw Z. Tomczuk. *Linear Synchronous Motors*. 2nd. Boca Raton: CRC Press, 2012, p. 520. ISBN: 978-1-4398-4221-8.

[32] M. Glinka. “Prototype of multiphase modular-multilevel-converter with 2 MW power rating and 17-level-output-voltage”. In: *2004 IEEE 35th Annual Power Electronics Specialists Conference (IEEE Cat. No.04CH37551)*. Vol. 4. 2004, 2572–2576 Vol.4. DOI: 10.1109/PESC.2004.1355234.

[33] Yoshimi Goda. *Random seas and design of maritime structures*. Vol. 33. World Scientific Publishing Company, 2010.

[34] Guanjun Ding et al. “New technologies of voltage source converter (VSC) for HVDC transmission system based on VSC”. In: *2008 IEEE Power and Energy Society General Meeting - Conversion and Delivery of Electrical Energy in the 21st Century*. 2008, pp. 1–8. DOI: 10.1109/PES.2008.4596399.

[35] Kester Gunn and Clym Stock-Williams. “Quantifying the global wave power resource”. In: *Renewable Energy* 44 (2012), pp. 296–304.

[36] Xue Han et al. “Transient Characteristics Under Ground and Short-Circuit Faults in a ±500 kV MMC-Based HVDC System With Hybrid DC Circuit Breakers”. In: *IEEE Transactions on Power Delivery* 33.3 (2018), pp. 1378–1387. DOI: 10.1109/TPWRD.2018.2795800.

[37] W. H. Hayt and J. A. Buck. *Engineering electromagnetics*. 8th Editio. New York: McGraw-Hill, 2012, p. 593. ISBN: 9780073380667.

[38] F. Herrera et al. "Wave Energy Conversion: Overview and Control of a Permanent Magnet Linear Generator". In: *2019 IEEE CHILEAN Conference on Electrical, Electronics Engineering, Information and Communication Technologies (CHILECON)*. Nov. 2019, pp. 1–6. DOI: 10.1109/CHILECON47746.2019.8988042.

[39] Neil Hodgins et al. "Design and Testing of a Linear Generator for Wave-Energy Applications". In: *IEEE Transactions on Industrial Electronics* 59.5 (2012), pp. 2094–2103. DOI: 10.1109/TIE.2011.2141103.

[40] Yue Hong et al. "Review on electrical control strategies for wave energy converting systems". In: *Renewable and Sustainable Energy Reviews* 31 (2014), pp. 329–342.

[41] Wei Huang and Jinming Yang. "A Novel Piecewise Velocity Control Method Using Passivity-Based Controller for Wave Energy Conversion". In: *IEEE Access* 8 (2020), pp. 59029–59043. DOI: 10.1109/ACCESS.2020.2982973.

[42] International Renewable Energy Agency (IRENA). *Renewable Capacity Statistics 2021*. en. URL: https://www.irena.org/publications/2021/March/Renewable-Capacity-Statistics-2021 (visited on 10/01/2021).

[43] M. Jama and A. Wahyudie. "Online Damping Strategy for Controlling Heaving Wave Energy Converters Using Three-Phase Bridge Boost Rectifier". In: *IEEE Access* 5 (2017), pp. 7682–7691.

[44] Abdulrahman Jbaily and Ronald W Yeung. "Piezoelectric devices for ocean energy: a brief survey". In: *Journal of Ocean Engineering and Marine Energy* 1.1 (2015), pp. 101–118.

[45] Jiabin Wang, G. W. Jewell, and D. Howe. "A general framework for the analysis and design of tubular linear permanent magnet machines". In: *IEEE Transactions on Magnetics* 35.3 (1999), pp. 1986–2000.

[46] Jih-Sheng Lai and Fang Zheng Peng. "Multilevel converters-a new breed of power converters". In: *IEEE Transactions on Industry Applications* 32.3 (1996), pp. 509–517. DOI: 10.1109/28.502161.

[47] Lawrence E Jones. *Renewable energy integration: practical management of variability, uncertainty, and flexibility in power grids*. Academic Press, 2014.

[48] J. F. Kelly et al. "Implementation and Verification of a Wave-to-Wire Model of an Oscillating Water Column With Impulse Turbine". In: *IEEE Transactions on Sustainable Energy* 7.2 (Apr. 2016), pp. 546–553.

[49] O. Keysan et al. "Designing the c-gen lightweight direct drive generator for wave and tidal energy". In: *IET Renewable Power Generation* 6.3 (May 2012), pp. 161–170.

[50] Muhammed Zafar Ali Khan, Haider Ali Khan, and Muhammad Aziz. "Harvesting Energy from Ocean: Technologies and Perspectives". In: *Energies* 15.9 (2022). ISSN: 1996-1073. DOI: 10.3390/en15093456. URL: https://www.mdpi.com/1996-1073/15/9/3456.

[51] J. S. Kim et al. "The development of detent force minimizing permanent magnet linear generator for direct-drive wave energy converter". In: *2012 Oceans*. 2012, pp. 1–7.

[52] J. Lekube, A. J. Garrido, and I. Garrido. "Rotational Speed Optimization in Oscillating Water Column Wave Power Plants Based on Maximum Power Point Tracking". In: *IEEE Transactions on Automation Science and Engineering* 14.2 (Apr. 2017), pp. 681–691.

[53] L. Li et al. "Wave Force Prediction Effect on the Energy Absorption of a Wave Energy Converter With Real-Time Control". In: *IEEE Transactions on Sustainable Energy* 10.2 (Apr. 2019), pp. 615–624.

[54] Yonggang Lin et al. "Review of hydraulic transmission technologies for wave power generation". In: *Renewable and Sustainable Energy Reviews* 50 (2015), pp. 194–203.

[55] Iraide López et al. "Review of wave energy technologies and the necessary power-equipment". In: *Renewable and Sustainable Energy Reviews* 27 (2013), pp. 413–434.

[56] Aquatera ltd. *Recommendations for Chile's Marine Energy Strategy: a roadmap for development*. Mar. 2014. URL: https://www.gov.uk/government/publications/recommendations-for-chiles-marine-energy-strategy.

[57] Aleix Maria-Arenas et al. "Control Strategies Applied to Wave Energy Converters: State of the Art". In: *Energies* 12.16 (2019). ISSN: 1996-1073. DOI: 10.3390/en12163115. URL: https://www.mdpi.com/1996-1073/12/16/3115.

[58] R. Marquardt. "Modular Multilevel Converter: An universal concept for HVDC-Networks and extended DC-Bus-applications". In: *The 2010 International Power Electronics Conference - ECCE ASIA -*. 2010, pp. 502–507. DOI: 10.1109/IPEC.2010.5544594.

[59] Mehmet Melikoglu. "Current status and future of ocean energy sources: A global review". In: *Ocean Engineering* 148 (2018), pp. 563–573.

[60] H. Mendonca and S. Martinez. "A resistance emulation approach to optimize the wave energy harvesting for a direct drive point absorber". In: *IEEE Transactions on Sustainable Energy* 7.1 (Jan. 2016), pp. 3–11.

[61] L. D. Mesantono, F. Danang Wijaya, and T. Haryono. "Comparison of linear flux permanent magnet generator topologies by using FEMM 2D". In: *2016 8th International Conference on Information Technology and Electrical Engineering (ICITEE)*. 2016, pp. 1–5.

[62] Bisni Fahad Mon et al. "Adaptive Maximum Power Point Tracking Algorithm for Heaving Wave Energy Converters". In: *OCEANS 2019 - Marseille*. 2019, pp. 1–5. DOI: 10.1109/OCEANSE.2019.8867039.

[63] Vito G. Monopoli et al. "Applications and Modulation Methods for Modular Converters Enabling Unequal Cell Power Sharing: Carrier Variable-Angle Phase-Displacement Modulation Methods". In: *IEEE Industrial Electronics Magazine* 16.1 (2022), pp. 19–30. DOI: 10.1109/MIE.2021.3080232.

[64] Nicolás Müller et al. "Medium-Voltage Power Converter Interface for Multigenerator Marine Energy Conversion Systems". In: *IEEE Transactions on Industrial Electronics* 64.2 (2017), pp. 1061–1070. DOI: 10.1109/TIE.2016.2615276.

[65] A. Nami et al. "Five level cross connected cell for cascaded converters". In: *2013 15th European Conference on Power Electronics and Applications (EPE)*. 2013, pp. 1–9. DOI: 10.1109/EPE.2013.6631941.

[66] António F. de O. Falcão. "Wave energy utilization: A review of the technologies". In: *Renewable and Sustainable Energy Reviews* 14.3 (2010), pp. 899–918.

[67] Juan David Páez et al. "Overview of DC–DC Converters Dedicated to HVdc Grids". In: *IEEE Transactions on Power Delivery* 34.1 (2019), pp. 119–128. DOI: 10.1109/TPWRD.2018.2846408.

[68] Joon Sung Park et al. "Active Phase Control for Maximum Power Point Tracking of a Linear Wave Generator". In: *IEEE Transactions on Power Electronics* 32.10 (2017), pp. 7651–7662. DOI: 10.1109/TPEL.2016.2625843.

[69] Arthur Pecher and Jens Peter Kofoed. *Handbook of ocean wave energy*. Springer London, 2017.

[70] Markel Penalba, Giussepe Giorgi, and John V. Ringwood. "Mathematical modelling of wave energy converters: A review of nonlinear approaches". In: *Renewable and Sustainable Energy Reviews* 78 (2017), pp. 1188–1207.

[71] Marcelo A. Perez et al. "Circuit Topologies, Modeling, Control Schemes, and Applications of Modular Multilevel Converters". In: *IEEE Transactions on Power Electronics* 30.1 (2015), pp. 4–17. DOI: 10.1109/TPEL.2014.2310127.

[72] H. Polinder, M. E. C. Damen, and F. Gardner. "Linear PM Generator system for wave energy conversion in the AWS". In: *IEEE Transactions on Energy Conversion* 19.3 (Sept. 2004), pp. 583–589. ISSN: 1558-0059. DOI: 10.1109/TEC.2004.827717.

[73] Safdar Rasool et al. "An Advanced Control Strategy for a Smooth Integration of Linear Generator Based Wave Energy Conversion System with Distribution Power Grids". In: *2019 IEEE Industry Applications Society Annual Meeting*. 2019, pp. 1–6. DOI: 10.1109/IAS.2019.8912314.

[74] REN21. *Renewables 2019: Global Status Report*. Tech. rep. Paris: Renewable Energy Policy Network for the 21st Century, 2019, pp. 1–335. URL: http://www.ren21.net/gsr-2019/.

[75] REN21. *Renewables 2021 Global Status Report (https://www.ren21.net/reports/global-status-report/)*. Tech. rep. Paris: REN21 Secretariat: Renewable Energy Policy Network for the 21st Century, 2021, pp. 1–370. URL: https://www.ren21.net/reports/global-status-report/.

[76] O. Saeed et al. "Simple Resonance Circuit to Improve Electrical Power Conversion in a Two-Sided Planar Permanent Magnet Linear Generator for Wave Energy Converters". In: *IEEE Access* 5 (2017), pp. 18654–18664.

[77] E. V. Sánchez, R. H. Hansen, and M. M. Kramer. "Control Performance Assessment and Design of Optimal Control to Harvest Ocean Energy". In: *IEEE Journal of Oceanic Engineering* 40.1 (Jan. 2015), pp. 15–26.

[78] K. Sharifabadi et al. "Introduction to Modular Multilevel Converters". In: *Design, Control, and Application of Modular Multilevel Converters for HVDC Transmission Systems*. 2016, pp. 7–59. DOI: 10.1002/9781118851555.ch1.

[79] J.K.H. Shek, D.E. Macpherson, and M.A. Mueller. "Power conversion for wave energy applications". In: *IET Conference Proceedings* (Jan. 2010), 242–242(1).

[80] W. Sheng and A. Lewis. "Power Takeoff Optimization for Maximizing Energy Conversion of Wave-Activated Bodies". In: *IEEE Journal of Oceanic Engineering* 41.3 (July 2016), pp. 529–540.

[81] Gavin Smart and Miriam Noonan. *Tidal Stream and Wave Energy Cost Reduction and Industrial Benefit: Summary Analysis*. Tech. rep. Catapult, 2018, p. 21.

[82] E. Solas et al. "Modular Multilevel Converter With Different Submodule Concepts—Part I: Capacitor Voltage Balancing Method". In: *IEEE Transactions on Industrial Electronics* 60.10 (2013), pp. 4525–4535. DOI: 10.1109/TIE.2012.2210378.

[83] E. Solas et al. "Modular Multilevel Converter With Different Submodule Concepts—Part II: Experimental Validation and Comparison for HVDC Application". In: *IEEE Transactions on Industrial Electronics* 60.10 (2013), pp. 4536–4545. DOI: 10.1109/TIE.2012.2211431.

[84] Peter Tavner. *Wave and Tidal Generation Devices: Reliability and Availability*. Vol. 2. IET, 2017.

[85] N. Thitichaiworakorn, M. Hagiwara, and H. Akagi. "Experimental Verification of a Modular Multilevel Cascade Inverter Based on Double-Star Bridge Cells". In: *IEEE Transactions on Industry Applications* 50.1 (2014), pp. 509–519. DOI: 10.1109/TIA.2013.2269896.

[86] Juanjuan Wang, Zhongxian Chen, and Fei Zhang. "A Review of the Optimization Design and Control for Ocean Wave Power Generation Systems". In: *Energies* 15.1 (2022). ISSN: 1996-1073. DOI: 10.3390/en15010102. URL: https://www.mdpi.com/1996-1073/15/1/102.

[87] Liguo Wang, Jan Isberg, and Elisabetta Tedeschi. "Review of control strategies for wave energy conversion systems and their validation: the wave-to-wire approach". In: *Renewable and Sustainable Energy Reviews* 81 (2018), pp. 366–379.

[88] *Wave devices : EMEC: European Marine Energy Centre*. URL: https://www.emec.org.uk/marine-energy/wave-devices/ (visited on 10/08/2021).

[89] A. Whiteman et al. "Total capacity from International Renewable Energy Agency". In: *Renewable Capacity Statistics 2019* (Mar. 2019), p. 60.

[90] T. Xia et al. "Design and Analysis of a Field-Modulated Tubular Linear Permanent Magnet Generator for Direct-Drive Wave Energy Conversion". In: *IEEE Transactions on Magnetics* 53.6 (June 2017), pp. 1–4.

[91] T. Xia et al. "Research on the Field-Modulated Tubular Linear Generator With Quasi-Halbach Magnetization for Ocean Wave Energy Conversion". In: *IEEE Transactions on Applied Superconductivity* 28.3 (Apr. 2018), pp. 1–5. ISSN: 1051-8223. DOI: 10.1109/TASC.2018.2797959.

[92] X. Xiao, X. Huang, and Q. Kang. “A Hill-Climbing-Method-Based Maximum-Power-Point-Tracking Strategy for Direct-Drive Wave Energy Converters”. In: *IEEE Transactions on Industrial Electronics* 63.1 (Jan. 2016), pp. 257–267.

[93] Xi Xiao, Xuanrui Huang, and Qing Kang. “A Hill-Climbing-Method-Based Maximum-Power-Point-Tracking Strategy for Direct-Drive Wave Energy Converters”. In: *IEEE Transactions on Industrial Electronics* 63.1 (2016), pp. 257–267. DOI: 10.1109/TIE.2015.2465964.

[94] H. M. Zapata et al. “Model of a permanent magnet linear generator”. In: *IECON 2019 - 45th Annual Conference of the IEEE Industrial Electronics Society*. Vol. 1. 2019, pp. 6992–6997.

[95] Henry M. Zapata, Marcelo A. Perez, and Abraham Marquez Alcaide. “Control of Cascaded Multilevel Converter for Wave Energy Applications”. In: *Energies* 16.1 (2023). ISSN: 1996-1073. DOI: 10.3390/en16010071. URL: https://www.mdpi.com/1996-1073/16/1/71.

[96] Henry M. Zapata and Marcelo A. Pérez. “Modular Multilevel Converter for a Linear Generator for Wave Energy Converter”. In: *Energies* 15.17 (2022). ISSN: 1996-1073. DOI: 10.3390/en15176346. URL: https://www.mdpi.com/1996-1073/15/17/6346.

[97] Jing Zhang et al. “Design and Experimental Analysis of AC Linear Generator with Halbach PM Arrays for Direct-Drive Wave Energy Conversion”. In: *IEEE Transactions on Applied Superconductivity* 24.3 (2014), pp. 3–6. ISSN: 10518223. DOI: 10.1109/TASC.2013.2292640.